Tumor necrosis factor (TNF)-α is a potential trigger of neural cell injury in the spinal cord.[9-11] TNF-α mediates several biologic and immunoregulatory responses in a variety of inflammatory diseases and trauma of the central nervous system including the spinal cord.[12-15] It is highly possible that both TNF receptor 1 (TNFR1) and TNF receptor 2 (TNFR2), both members of the TNFR superfamily,[16,17] are involved in these potentially destructive cellular reactions mediated by TNF-α. In a chronic spinal cord compression model, we showed that TNF-α, TNFR1, and TNFR2 induced neuronal and oligodendroglial cell apoptosis after spinal cord injury.[18] The biologic activity of TNF-α is inhibited by the TNF-α antagonist etanercept, which has demonstrated efficacy in rheumatoid and psoriatic arthritis by reducing joint inflammation and pain.[19-21] Etanercept inhibits TNF activity by competitive binding for cell-surface receptor interactions. It binds to TNF-α and TNF-β, in a reversible fashion, and after dissociation, the TNF remains bioactive. Etanercept also reduces secondary inflammatory damage to the spinal cord after traumatic injury.[22,23] However, it remains unknown how etanercept suppresses neuronal and oligodendroglial apoptosis in spinal cord injury.

This study investigated the effects and possible mechanisms of action of etanercept in the rat spinal cord contusion model, with a particular focus on the inhibition of TNF-α-mediated neuronal and oligodendroglial apoptosis. To our knowledge, this is the first experimental investigation of etanercept on neuronal function and neurologic improvement after spinal cord injury.

MATERIALS AND METHODS

Animal Model of Spinal Cord Injury

Experiments were conducted in 108 adult male Sprague-Dawley rats (Clea, Tokyo, Japan), aged 8 to 10 weeks with a mean body weight of 275 ± 35.2 g (±SD). After anesthesia by intraperitoneal injection of sodium pentobarbiturate (0.05 mg/g body weight), laminectomy was performed at the T9 and T10 levels using a surgical microscope (VANOX-S, Olympus, Tokyo, Japan), taking utmost care to avoid damaging the dura mater. The dorsal surface of the spinal cord was compressed extradurally at the T10 cord level using a 90-g static load (custom-made rod, 2 × 3 mm in diameter) for 2 minute, as described previously.[8] In one group of rats were treated by intraperitoneal administration of etanercept at the dosage of 5 mg/kg 1 hour after the contusion (n = 45). In the other group of rats with the same magnitude of spinal cord injury (n = 45), 1 mL of saline was injected 1 hour after the contusion injury: these animals served as the control group.[23] Rats subjected to laminectomy, but with no spinal cord injury sustained, served as the sham-operated group (n = 18). After surgery, all animals were housed under a 12-hour light-dark cycle in a bacteria free biologically clean room with access to food and water *ad libitum*.

This study was carried out in the Orthopaedic Spinal Cord Laboratort of University of Fukui. The experimental protocol strictly followed the Ethics Review Committee Guidelines for Animal Experimentation of our University.

Immunoblot Analysis

Immunoblot analysis was performed at 6 hour, 12 hour, 1 day, 3 day, 1 week, and 2 week after spinal cord injury using the method described previously by our group.[8,18,24] Immediately after anesthesia by intraperitoneal injection of sodium pentobarbiturate, the damaged spinal cord around the epicenter of the lesion (longitudinal section approximately 20 mm in length) was dissected *en bloc* from the spine and stored immediately at −80°C in liquid nitrogen. Sections were centrifuged at 15,000*g* for 30 second using a BioMasher Rapid Homogenization Kit (Funakoshi Co Ltd, Tokyo, Japan). Samples were then solubilized in RIPA buffer [50 mmol/L Tris-HCl, pH 7.5, 150 mmol/L NaCl, 1% Triton X-100, 0.5% sodium deoxycholate, 20 μg/mL leupeptin, and 1 mmol/L phenylmethylsulfonylfluoride (PMSF)], homogenized, and stored at −80°C. Protein concentration was determined by a DC Protein Assay Kit (Bio-Rad Laboratories, Hercules, CA). Laemmli sodium dodecylsulfate buffer samples containing the protein mixtures were boiled and subjected to immunoblot analysis. Total protein (20 μg/lane) was separated on 12.5% SDS-PAGE and transferred onto polyvinylidene difluoride membrane (PE Applied Biosystems, Foster, CA) for 70 minute using a semidry blot apparatus. The membrane was washed twice in phosphate-buffered saline (PBS) containing 0.05% Tween 20, blocked by 5% skim milk in PBS for 1 hour at room temperature, and then incubated with either anti-TNF-α (code No. Ab9755, 1:500, rabbit IgG, Abcam plc, Cambridge, UK), anti-TNFR1 (code No. SC7895, 1:200, rabbit IgG; Santa Cruz Biotechnology, Santa Cruz, CA), anti-TNFR2 (code No. SC7862, 1:200, rabbit IgG; Santa Cruz Biotechnology), antiactive caspase-3 polyclonal antibody (code No. Ab2302, 1:200, rabbit IgG; Abcam plc), and anticaspase-8 polyclonal antibody (code No. Ab52183, 1:200, rabbit IgG; Abcam plc) overnight at 4°C, followed sequentially by antirabbit or antimouse IgG antibody and avidin-biotinylated peroxidase complex (1:10000; Envision System-HRP Labeled Polymer, Dako Cytomation, Carpenteria, CA) for 30 minutes each. After triple washing in 0.1 M PBS, the membrane was immersed in a chemiluminescence reagent for 1 minute and then subjected to radiography to visualize the peroxidase activity and thus level of antibody binding. The band intensities of TNF-α, TNFR1, TNFR2, and active-caspase-3 and caspase-8 were normalized to β-actin (code No. IMG-5142A, 1:1000, rabbit IgG, Imgenex, San Diego, CA).

Immunofluorescence Staining and Double Staining

At 6 hour, 12 hour, 1 day, 3 day, 1 week, and 2 week after spinal cord injury, animals were reanesthetized and 300 mL of PBS was perfused intracardially followed by 200 mL of 2% paraformaldehyde in 0.1 M PBS (pH 7.6). Immediately after perfusion, the spinal cord from T8–T12 cord segments was removed *en bloc* and stored in 0.1 M PBS containing 20% sucrose at 4°C for 36 hour. Tissue blocks were embedded in Tissue-Tek [optimal cutting temperature (OCT) compound 4583; Sakura Finetechnical, Tokyo, Japan), frozen, and then stored at −80°C. Three sham-operated rats that underwent laminectomy without compression were also killed

and processed for the other groups. Using a cryostat, serial 25-μm-thick transverse frozen sections were prepared for immunofluorescence staining. All sections were serially mounted on glass slides and fixed with 2% paraformaldehyde in 0.1 M PBS for 5 minutes, rinsed in PBS, and then stored at −20°C. Serial 25-μm-thick transverse frozen sections were also treated with 0.1 M Tris-HCl buffer (pH 7.6) containing 0.3% Triton-X-100 for another 24 hour to allow reaction of the cell membrane with the antibodies. Sections were incubated at 4°C overnight with anti-TNF-α antibody (code No. SC1348, 1:100, gout IgG; Santa Cruz Biotechnology), anti-TNFR1 antibody (code No. SC7895, 1:100, rabbit IgG; Santa Cruz Biotechnology), or anti-TNFR2 antibody (code No. SC7862, 1:100, rabbit IgG; Santa Cruz Biotechnology) diluted in Antibody Diluent with Background Reducing Components (Dako Cytomation, Carpinteria, CA). The secondary antibody was goat antirabbit Alexa Flour 488-conjugated antibody (1:250; Molecular Probes, Eugene, OR), applied for 1 hour at room temperature.

For double immunofluorescence staining, the sections were further incubated with antineuronal nuclei monoclonal antibody (code No. MAB377, NeuN, 1:100, mouse IgG; Chemicon International, Temecula, CA), antioligodendrocyte monoclonal antibody (code No. MAB1580, RIP, 1:100, mouse IgG; Chemicon International), antimacrophage monoclonal antibody (code No. Ab1211, OX-42, 1:100, CD11b, Abcam plc), or antiglial fibrillary acidic protein monoclonal antibody (code No. G3893, 1:100, mouse IgG; σ-Aldrich Co., St Louis, MO) diluted in Antibody Diluent with Background Reducing Components (Dako Cytomation) at 4°C overnight. The sections were then incubated with goat antimouse Alexa Flour 568-conjugated antibody (1:250; Molecular Probes). The immunostained cells were visualized under a fluorescent microscope (Olympus AX80, Tokyo, Japan) or confocal microscope equipped with a 15-mW krypton argon laser (model TCS SP2, Leica Instruments, Nussloch, Germany). The 488- and 568-nm lines of the argon/helium-neon laser were used for fluorescence excitation.

Histology and Measurement of Cystic Cavities

Sections of the spinal cord were also taken at the same earlier-mentioned time course of immunohistochemistry after intracardial perfusion with PBS and 4% paraformaldehyde. Sections were fixed for 24 hour in 4% paraformaldehyde solution at 4°C, dehydrated through a graded ethanol series, and embedded in paraffin. Tissue sections (10-μm thick) were deparaffinized in xylene and stained with luxol fast blue (LFB) and with hematoxylin and eosin (HE). For a semiquantitative analysis of demyelination, lesion areas were cross-referenced with the HE staining to establish cellularity. The axial 10 random sections within 1500 μm rostral and caudal to the epicenter were examined using standard brightfield microscopy. At 2 week, 4 week, and 8 week after spinal cord injury, LFB-positive areas in ventrolateral funiculus were analyzed under 400× magnification using grain counting with the light intensity automatically set by a color image analyzer (MacSCOPE; Mitani, Fukui, Japan). LFB-positive area in which the density significantly exceeded the threshold of each background was calculated as percentage cross-sectional area of residual tissue.[25]

Assessment of Locomotor Behavior

To assess the behavior of each rat after spinal contusion and recovery of locomotor function, 48 rats from each group [the control (injected with saline), etanercept-treated, and sham-operated groups] were investigated at 1 day, 3 day, 1 week, 2 week, 4 week, and 8 week after administration of saline or etanercept. Locomotor function of the hind limbs was graded using the Basso-Beattie-Bresnahan (BBB) hind limb locomotor rating scale.[26] The BBB rating scale is a 21-point system on the basis of operationally defined behavioral features, which follow the recovery progression from complete paralysis to normal locomotion. The rating scale ranges from 0 to 21, with a score of 0 indicating complete hind limb paralysis, whereas a score of 21 denotes completely normal locomotor function. Scores of 0 to 20 indicate an animal's altered ability to move the hind limb joints, to bear weight, and to coordinate forelimb and hind limb movement.

Terminal Deoxynucleotidyl Transferase (TdT)-Mediated dUTP-Biotin Nick End Labeling (TUNEL) Staining

Serial 25-μm-thick transverse frozen sections were prepared for TUNEL staining as for immunofluorescence staining. Deoxyribonucleic acid fragmentation was detected by the TUNEL method using the ApopTag Peroxidase *in situ* Apoptosis Detection kit (Chemicon International). The experiments were performed as described in the kit manual. The reaction with TdT was terminated by washing the sections with stop-wash buffer for 10 minute at room temperature. Antidigoxigenin peroxidase was then applied for 30 minute at room temperature, and then the sections were incubated with antineuronal nuclei monoclonal antibody (code No. MAB377, NeuN, 1:100, mouse IgG; Chemicon International) and antioligodendrocyte monoclonal antibody (code No. MAB1580, RIP, 1: 100, mouse IgG; Chemicon International) diluted in Antibody Diluent with Background Reducing Components at 4°C overnight. Goat antimouse Alexa Flour 568/fluorescein-conjugated secondary antibody (1: 250; Molecular Probes) was subsequently applied. To quantitatively examine the numbers of apoptotic cells, TUNEL-positive cells at each time point were counted in 20 random sections between 5 mm and 10 mm rostral and caudal to the injury epicenter, respectively on gray matter and white matter of sections from control and etanercept-treated animals with a color image analyzer (MacSCOPE). The average number of sections labeled with TUNEL (green) was calculated throughout the lesion site of each animal. The number of TUNEL-positive cells in which the density significantly exceeded the threshold in each background calculated in sham-operated rats in each gray and white matter was counted.[27] The immunostained cells were also visualized by confocal microscopy.

Statistical Analysis

All values are expressed as mean ± SD. Differences between groups were examined for statistical significance using the

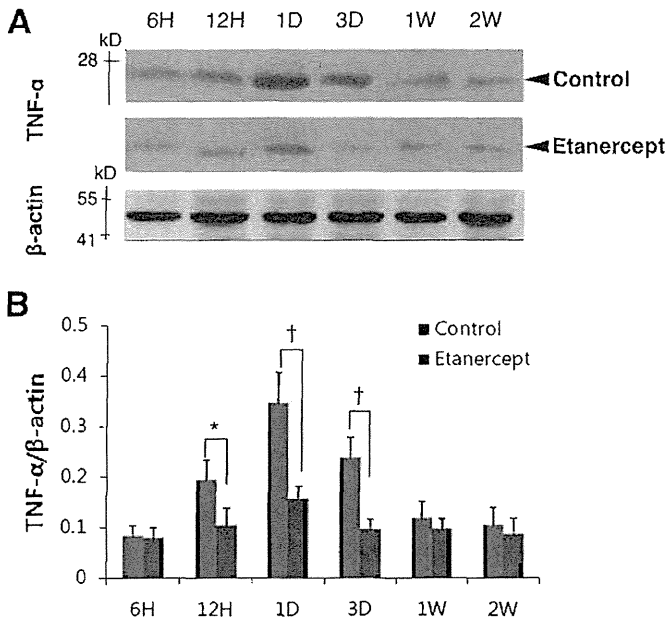

Figure 1. A, Immunoblot analysis of TNF-α expressions in saline groups (control) and etanercept-treated groups. B, Graphs indicate relative band intensities compared with that of β-actin. The relative expression in the etanercept-treated group was weaker than those in the control animals, especially in the acute phase (12 hours, 1 day, 3 day) after spinal cord injury compared (B: n = 3 for each time point).

paired *t* test. A $P < 0.05$ denoted the presence of a significant difference. The above tests were conducted using SPSS software version 11.0 (SPSS, Chicago, IL).

RESULTS

Temporal Pattern of Inflammatory Cytokine Expression with or Without Etanercept Administration

Differences in TNF-α expression in the injured spinal cord were assessed by immunoblot analysis with or without etanercept administration at several time points after spinal cord injury (Figure 1A). The highest expression of TNF-α was observed at 1 day after cord injury. Administration of etanercept significantly suppressed the TNF-α expression at 12 hour, 1 day, and 3 day after cord injury (Figure 1B). Next, we evaluated the cellular expression of TNF-α pathway components by double immunofluorescent staining using TNF-α/NeuN (for neurons), TNF-α/OX-42 (for macrophages), TNF-α/GFAP (for astrocytes), and TNFR1/RIP and TNFR2/RIP (for oligodendrocytes). Spinal cord injury resulted in the induction of TNF-α expression in neurons, oligodendroglia, microglia, and astroglial cells at 1 day after the cord injury (Figure 2 upper row, control) at an adjacent section of epicenter. Etanercept treatment suppressed the expression of TNF-α in all neurons and glial cells (Figure 2; lower row).

Cellular Expression of the TNF-α/TNFR Pathway in Injured Spinal Cord

Differences in expressions of TNFR1 and TNFR2 between control groups and etanercept-administered groups were investigated by immunoblot analysis (Figure 3A). Overexpression of TNFR1 and TNFR2 was evident in the injured spinal cord at 6 and 12 hour after the contusion injury in control animals, whereas in the etanercept-treated group, the immunoreactivity was decreased for TNFR1 at 6 and 12 hour and for TNFR2 at 6 hour after injury (Figure 3B, C).

Double-stained sections for TNFR1 and TNFR2 with neural and oligodendroglial cell marker revealed markedly reduced coexpression of TNFR1 and TNFR2 with NeuN in the gray matter or RIP in the white matter at 6 hour after injury in etanercept-treated animals at 5 mm rostral to the epicenter (Figure 4).

Histologic Evaluation of the Injured Spinal Cord

The severity of trauma at the injury epicenter site was evaluated in both groups. Axial samples of the spinal cord were evaluated at each time point using HE and LFB staining. HE staining (Figure 5A) showed a significant decrease in neural injury with etanercept treatment (right column panels) compared to controls; edema was also reduced and structural preservation of the spinal cord was enhanced. Cystic formation was weak in the etanercept group at 2, 4, and 8 week after injury. In LFB-stained samples, while at 2, 4, and 8 week, images demonstrated significantly smaller areas of

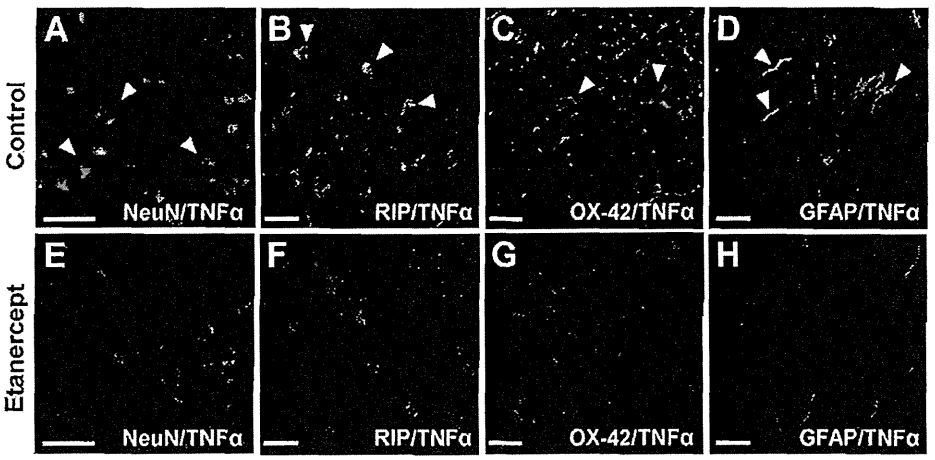

Figure 2. Photomicrograph showing the colocalization of cell-specific markers (red) and TNF-α (green) in saline groups and etanercept-administered groups at 1 day after spinal cord injury at 5 mm rostral to the injury epicenter. Expression of TNF-α was significant in neurons (NeuN: A), oligodendroglia (RIP: B), microglia (OX-42: C), and astroglial cells (GFAP: D) in control. In the etanercept-treated group (E–H), numbers of all double-positive cells (yellow) were significantly decreased. Arrowheads indicate colocalization of the cell-specific marker and TNF-α. Scale bar = 50 μm (A, E), 10 μm (B–D, F–H).

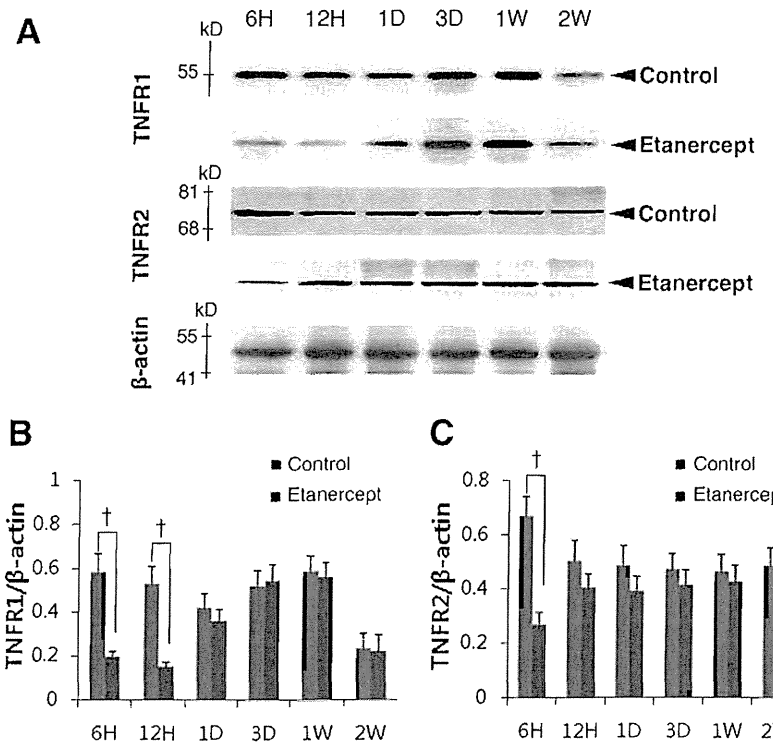

Figure 3. A, Immunoblot analysis of TNFR1 and TNFR2 expression at several time intervals after spinal cord injury. Graphs indicate relative band intensity compared with that of β-actin (**B**, **C**: n = 3 for each time point). TNFR1 expression was significantly low in the treatment group at 6- and 12-hour postinjury compared to the controls. TNFR2 expression was also reduced in the etanercept-treated group at 6 hour compared to controls. The data are expressed as mean ± SD. $*P < 0.05$, $\dagger P < 0.01$, compared to β-actin.

cystic cavity formation and enhanced staining in both gray and white matters (Figure 5B, C). At the injury epicenter sites, the percentage cross-sectional area of residual tissue was significantly larger in the etanercept-treated group than in controls at 2 week, 4 week, and 8 week after spinal cord injury (Figure 5D).

Evaluation of Locomotor BBB Score

The degree of motor disturbance in the hind limbs was assessed at 1 day, 3 day, 1 week, 2 week, 4 week, and 8 week after spinal cord injury. Rats sustaining spinal cord injury had significant motor disturbances in the hind limb. Etanercept administration significantly increased the BBB locomotor score at 2, 4, and 8 week after the cord injury (Figure 6).

Effects of Etanercept on Neural and Glial Cell Apoptosis

Significant levels of TUNEL/NeuN and TUNEL/RIP double staining were evident in samples from the control group; whereas etanercept-treated animals showed fewer TUNEL/NeuN and TUNEL/RIP positive cells (Figure 7A, B). Counting of the TUNEL-positive cells in saline groups and etanercept-administered groups using a color image analyzer (MacSCOPE) showed significantly decreased numbers at 12 hour, 1 day, 3 day, and 1 week after the cord injury in the gray matters of etanercept-treated rats (Figure 7C), and at 12 hour, 1 day, 3 day, and 1 week in the white matters of etanercept-treated animals at the adjacent sites to the epicenter (Figure 7D).

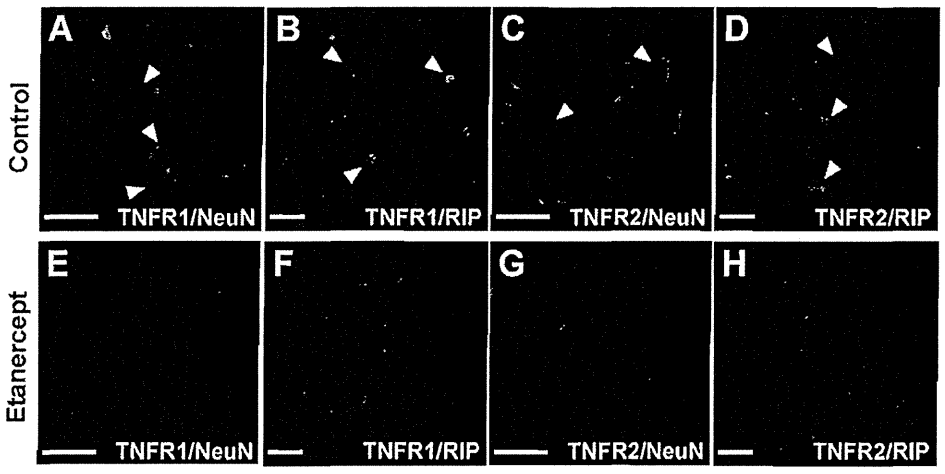

Figure 4. Photomicrograph showing colocalization of the cell marker (NeuN and RIP; red) with either TNFR1 or TNFR2 (green) in the control groups (**A–D**) and etanercept-treated (**E–H**) groups at 6 hour after spinal cord injury at 5 mm rostral to the epicenter. The expressions of both receptors on neurons in the gray matter and oligodendroglia in the white matter were markedly suppressed by etanercept administration. Arrowheads indicate colocalization (yellow) of the cell-specific marker and TNFR1 or TNFR2. Scale bar = 50 μm (**A, E**), 10 μm (**B–D, F–H**).

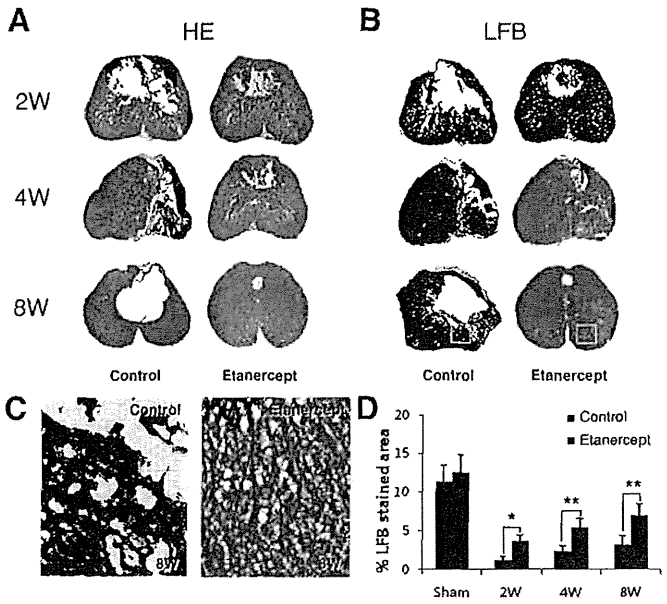

Figure 5. Histological evaluation of cord injury with HE (A) and LFB (B) staining. A, B, The etanercept group showed a lower degree of spinal cord tissue damage and edema than control groups at the injury epicenter. LFB staining of the ventral microcystic cavity at 8 week after cord injury (box area in B) showed a remarkable reduction in the area of demyelination in the etanercept-treated group compared with the control group (C). Percentage of cross-sectional area of residual tissue and cavitations at the injury epicenter sites represented from 2 to 8 week after spinal cord injury (D: n = 3 for each time point). An overall significant difference was found in the areas of residual tissue and cavitations ($P < 0.001$). The percentage cross-sectional area of residual tissue was significantly different between groups at each time point. *$P < 0.05$, †$P < 0.01$.

Next, we compared the protein expression levels of active caspase-3 and caspase-8 after etanercept administration. The band intensities for both active caspase-3 and caspase-8 in the etanercept group were relatively weaker than those in controls, particularly in the acute phase (6 hour, 12 hour, 1 day, and 3 day) after cord injury (Figure 8).

DISCUSSION

This study provided new insights on spinal cord injury by investigating the effect of TNF-α antagonist, etanercept, in the rat spinal cord injury. The main effects of etanercept demonstrated herein were as follows: (1) reduction of TNF-α, TNFR1, and TNFR2 overexpression, especially in neurons and oligodendroglia in the acute phase of spinal cord injury; (2) prevention of tissue damage and demyelination in the spinal cord 2 week after the cord injury and thereafter; (3) increase in the locomotor BBB score in the hindlimb at 2 week and thereafter after injury; and (4) suppression of neuronal and oligodendroglial cell apoptosis in both gray and white matter of the spinal cord at the adjacent sites the injury epicenter. These findings indicated that etanercept could potentially play an important role in reducing neural damage of the spinal cord after traumatic injury *via* its suppressive actions on the TNF-mediated proinflammatory response

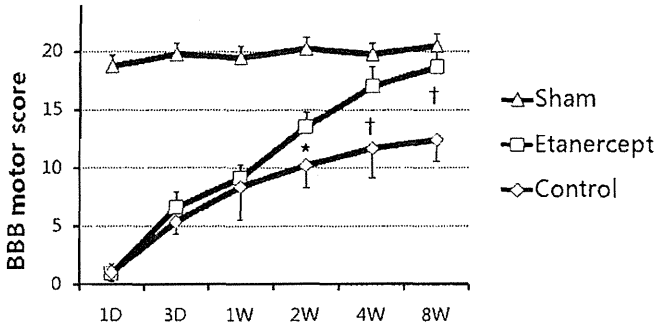

Figure 6. Analysis of locomotor BBB score after the cord injury. A significant improvement in hindlimb motor function was observed in the etanercept-treated group compared with the control groups from 2 week after the injury (n = 3 for each time point; n = 2 in sham-operated group). *$P < 0.05$, †$P < 0.01$.

and on apoptosis of neurons and oligodendroglia within the spinal cord.

The cascade of secondary tissue damage after spinal cord injury is accompanied by an inflammatory response marked

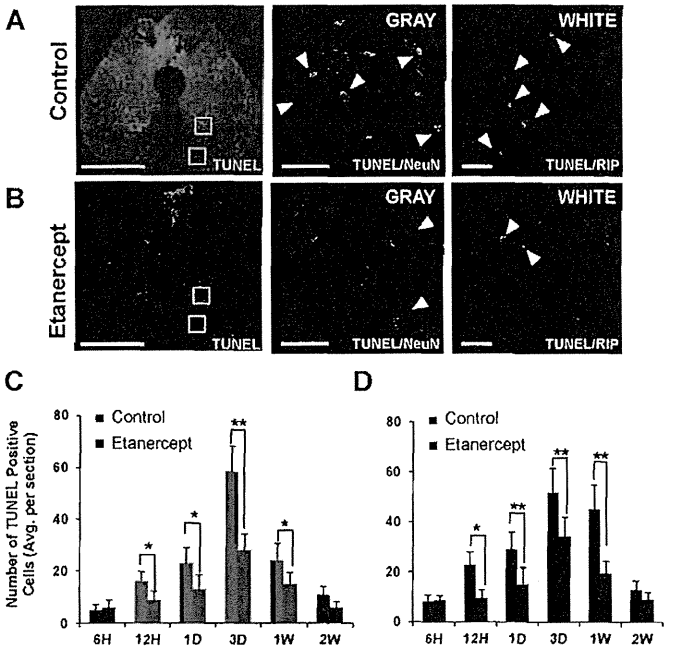

Figure 7. Representative TUNEL staining and the double immunofluorescence staining (box area in TUNEL staning) of TUNEL-positive cells (green) with NeuN or RIP (red) in control groups (A) and etanercept-treated (B) groups at 3 day after spinal cord injury at 5 mm rostral to the epicenter. Arrowheads indicate colocalization of TUNEL-positive cells and the cell-specific marker. In the etanercept-treated group (B), numbers of all double-positive cells (yellow) were significantly decreased. Bar graphs (C, D) represent the quantitative analysis of TUNEL-positive cells per cross section in the gray and white matters of both groups between 5 mm with 10 mm rostral and caudal to the injury epicenter (n = 3 for each time point). The number of TUNEL-positive neurons in the gray matter (C) and oligodendroglia in the white matter (D) was decreased in the etanercept-treated group at the adjacent site to the epicenter. Scale bars = 500 μm (left column), 50 μm (middle column), 10 μm (right column). Data are mean ± SD. *$P < 0.05$, †$P < 0.01$.

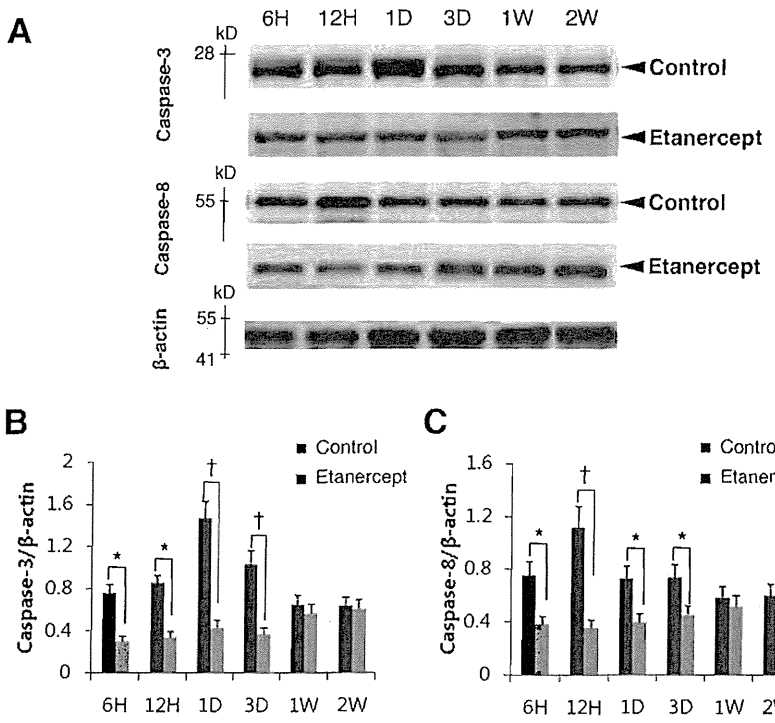

Figure 8. Immunoblot results showing expression of activated caspase-3 and caspase-8 at several time intervals after spinal cord injury (A). Graphs indicate relative band intensities compared with that of β-actin (B, C: n = 3 for each time point). The intensity of both activated caspase-3 and caspase-8 bands in the treatment group was significantly low at 6 hour, 12 hour, 1 day, and 3 day, compared to control animals. The data are expressed as mean ± SD. $*P < 0.05$, $\dagger P < 0.01$, compared to β-actin.

by infiltration of neutrophils and macrophages, activation of glial cells, and upregulated expression of proinflammatory cytokines.[28–30] Together, these factors lead to increased vascular permeability, edema, and degradation of the extracellular matrix. Proinflammatory cytokines including TNF-α, interleukin (IL)-1β, and IL-6 are involved in recruiting leukocytes and activating macrophages and microglia, and such cytokines are upregulated early in the inflammatory response.[31] These inflammatory cytokines, and particularly TNF-α, can initiate a large number of cellular responses including cytotoxicity, inflammation, immunoregulation, and transcriptional regulation of a large number of genes.[32] This study demonstrated that blocking the action of TNF-α decreased the magnitude of spinal cord tissue damage, reduced the extent of edema, and suppressed demyelination. Recently, Genovese *et al*[22] demonstrated that etanercept, reduced the expression of all these cytokines in a mouse model of spinal cord injury. Considered together, the present results and the above findings[22] suggest that TNF-α plays a detrimental role in the development and persistence of spinal cord injury and may in fact be one of the most important biologic triggers of the proinflammatory response in such cases.

Apoptotic neuronal and glial cells, including microglia, show overexpression of TNF-α in spinal cord injury, and it was suggested that TNF-α triggers oligodendroglial cell apoptosis, although the source of TNF-α in injured spinal cord was not identified.[33,34] A previous study also suggested that activated microglia secrete various cytotoxic factors including TNF-α in response to axonal regeneration and can therefore induce apoptosis of oligodendrocytes.[35] It was also reported that the population of apoptotic cells after spinal cord contusion injury comprises oligodendroglial cells, possibly phagocytic microglia or macrophages.[36] Double immunofluorescence staining in this study demonstrated the expression of TNF-α in not only microglia but also neurons, oligodendroglia, and reactive astroglia in the acute phase of spinal cord injury, and that etanercept seemed effective at suppressing TNF-α in all these cells. In addition, our results showed that etanercept suppressed the expression of both TNFR1 and TNFR2 in neurons and oligodendroglia.

TNF-α has been associated with degeneration of the remaining axons in the injury sites of spinal cords,[33] the promotion of myelin phagocytosis by macrophages,[37] and the death of the remaining oligodendrocytes capable of regenerating the myelin sheet. It has been considered that TNF-α eventually leads to a massive demyelination.[36] Etanercept is a dimeric fusion protein consisting of two extracellular domains of the human p75 TNF receptor, linked to the Fc portion of a type 1 human immunoglobulin (IgG1), which helps to retain the molecule in the circulation.[38] By competitive inhibition, the molecule of etanercept binds to two of the three receptor-binding sites on the TNF trimer; preventing TNF-α binding to the cell membrane receptors.[39] In this study, etanercept reduced the associated tissue damage of spinal cord injury and improved hindlimb locomotor function from 2 week after spinal cord injury. Our results may indicate that injection of etanercept after spinal cord injury leads to not only a delay of demyelination but also of the axonal degeneration at the injured site.

A variety of signal transduction pathways are involved in the complex process of apoptosis. Caspases are a family of cysteine proteases that are important in the effector phase of

apoptosis. Caspases are activated through intrinsic and extrinsic pathways. Spinal cord injury induces apoptosis *via* the activation of caspase-3[40] and increased expression of death receptors, especially Fas and p75 receptors.[41] On the contrary, the extrinsic pathway is initiated by ligands of cell-surface death receptors belonging to the TNF/nerve growth factor receptor superfamily.[42] The discovery and studies of a "death domain" in TNFR1 and related receptors revealed much about the signaling pathways mediating the activation of caspase-8 and caspase-3, before apoptosis.[43] It therefore seems reasonable to suggest that after a traumatic injury to the spinal cord, accumulation of TNF-α could initiate an apoptotic cascade *via* receptor-mediated signaling. Although TNFR1 mediates the majority of the apoptotic effects, whereas TNFR2 predominantly transmits cell-survival signals, their complete suite of locations and roles in TNF-α-induced signaling remains incomplete and controversial.[44] Holmes *et al*[17] localized the TNF receptors by immunocytochemistry; TNFR1 was found on neuronal cells and afferent fibers within the dorsal root ganglion, whereas TNFR2 immunoreactivity was absent in these locations. On the contrary, Yan *et al*[16] reported possible roles for TNFR1 and TNFR2 in adult rat spinal cord injury. These authors reported overexpression of TNFR1 and TNFR2 in the spinal cord and localized the receptors on neurons, astroglia, and oligodendroglia in spinal cord injury. Our results now indicate that suppression of both TNF-α receptors in the acute phase of spinal cord damage might inhibit apoptosis of neural and glial cells, whereas lifting the suppression of TNFR2 expression from 12 hour onward after the injury with TNF-α antagonist promoting regeneration of these same cells and contribute to a better recovery of locomotor function and decreased spinal cord tissue damage.

In conclusion, our results demonstrated that the administration of etanercept is likely to reduce the development of inflammatory tissue injury after spinal cord contusion. They also suggested that suppression of TNF-α/TNFR in the acute phase of cord injury by etanercept administration could contribute to inhibition of neuronal and glial cell apoptosis and promote better recovery of locomotor function.

➢ Key Points

- ❑ Expression of TNF-α, TNFR1, and TNFR2 in neurons and oligodendroglia in spinal cord injury could be suppressed by etanercept administration.
- ❑ Etanercept treatment induced an increased neurologic locomotor score, a decreased number of TUNEL-positive apoptotic neurons and oligodendroglia, and possibly myelination within 2 weeks after spinal cord injury.
- ❑ The current findings suggested that etanercept could improve spinal cord tissue damage, probably by suppressing TNF-α, TNFR1, TNFR2, and activated caspase-3 and caspase-8 expressions in the acute phase, and inhibiting the neuronal and oligodendroglial apoptosis caused by spinal cord injury.

References

1. Katoh K, Ikata T, Katoh S, et al. Induction and its spread of apoptosis in rat spinal cord after mechanical trauma. *Neurosci Lett* 1996;216:9–12.
2. Li GL, Brodin G, Farooque M, et al. Apoptosis and expression of Bcl-2 after compression trauma to rat spinal cord. *J Neuropathol Exp Neurol* 1996;55:280–9.
3. Crowe MJ, Bresnahan JC, Shuman SL, et al. Apoptosis and delayed degeneration after spinal cord injury in rats and monkeys. *Nat Med* 1997;3:73–6.
4. Nakahara S, Yone K, Sakou T, et al. Induction of apoptosis signal regulating kinase 1 (ASK1) after spinal cord injury in rats: possible involvement of ASK1-JNK and -p38 pathways in neuronal apoptosis. *J Neuropathol Exp Neurol* 1999;58:442–50.
5. Abe Y, Yamamoto T, Sugiyama Y, et al. Apoptotic cells associated with Wallerian degeneration after experimental spinal cord injury: a possible mechanism of oligodendroglial death. *J Neurotrauma* 1999;16:945–52.
6. Koda M, Murakami M, Ino H, et al. Brain-derived neurotrophic factor suppresses delayed apoptosis of oligodendrocytes after spinal cord injury in rats. *J Neurotrauma* 2002;19:777–85.
7. Tian DS, Xie MJ, Yu ZY, et al. Cell cycle inhibition attenuates microglia induced inflammatory response and alleviates neuronal cell death after spinal cord injury in rats. *Brain Res* 2007;1135:177–85.
8. . Nakajima H, Uchida K, Yayama T, et al. Targeted retrograde gene delivery of brain-derived neurotrophic factor suppresses apoptosis of neurons and oligodendroglia after spinal cord injury in rats. *Spine* 2010;35:497–504.
9. Yune TY, Chang MJ, Kim SJ, et al. Increased production of tumor necrosis factor-alpha induces apoptosis after traumatic spinal cord injury in rats. *J Neurotrauma* 2003;20:207–19.
10. Yune TY, Lee SM, Kim SJ, et al. Manganese superoxide dismutase induced by TNF-beta is regulated transcriptionally by NF-kappaB after spinal cord injury in rats. *J Neurotrauma* 2004;21:1778–94.
11. Profyris C, Cheema SS, Zang D, et al. Degenerative and regenerative mechanisms governing spinal cord injury. *Neurobiol Dis* 2004;15:415–36.
12. Feuerstein GZ, Liu T, Barone FC. Cytokines, inflammation, and brain injury: role of tumor necrosis factor-alpha. *Cerebrovasc Brain Metab Rev* 1994;6:341–60.
13. Arvin B, Neville LF, Barone FC, et al. The role of inflammation and cytokines in brain injury. *Neurosci Biobehav Rev* 1996;20:445–52.
14. Wang CX, Nuttin B, Heremans H, et al. Production of tumor necrosis factor in spinal cord following traumatic injury in rats. *J Neuroimmunol* 1996;69:151–6.
15. Bartholdi D, Schwab ME. Expression of pro-inflammatory cytokine and chemokine mRNA upon experimental spinal cord injury in mouse: an in situ hybridization study. *Eur J Neurosci* 1997;9:1422–38.
16. Yan P, Liu N, Kim GM, et al. Expression of the type 1 and type 2 receptors for tumor necrosis factor after traumatic spinal cord injury in adult rats. *Exp Neurol* 2003;183:286–97.
17. Holmes GM, Hebert SL, Rogers RC, et al. Immunocytochemical localization of TNF type 1 and type 2 receptors in the rat spinal cord. *Brain Res* 2004;1025:210–9.
18. Inukai T, Uchida K, Nakajima H, et al. Tumor necrosis factor-alpha and its receptors contribute to apoptosis of oligodendrocytes in the spinal cord of spinal hyperostotic mouse (twy/twy) sustaining chronic mechanical compression. *Spine* 2009;34:2848–57.
19. Moreland LW, Baumgartner SW, Schiff MH, et al. Treatment of rheumatoid arthritis with a recombinant human tumor necrosis factor receptor (p75)-Fc fusion protein. *N Engl J Med* 1997;337:141–7.
20. Seymour HE, Worsley A, Smith JM, et al. Anti-TNF agents for rheumatoid arthritis. *Br J Clin Pharmacol* 2001;51:201–8.
21. Catrina AI, Trollmo C, af Klint E, et al. Evidence that anti-tumor necrosis factor therapy with both etanercept and infliximab induces apoptosis in macrophages, but not lymphocytes, in rheumatoid arthritis joints: extended report. *Arthritis Rheum* 2005;52:61–72.
22. Genovese T, Mazzon E, Crisafulli C, et al. Immunomodulatory effects of etanercept in an experimental model of spinal cord injury. *J Pharmacol Exp Ther* 2006;316:1006–16.

23. Genovese T, Mazzon E, Crisafulli C, et al. Combination of dexamethasone and etanercept reduces secondary damage in experimental spinal cord trauma. *Neuroscience* 2007;150: 168–81.
24. Uchida K, Nakajima H, Inukai T, et al. Adenovirus-mediated retrograde transfer of neurotrophin-3 gene enhances survival of anterior horn neurons of twy/twy mice with chronic mechanical compression of the spinal cord. *J Neurosci Res* 2008;86: 1789–800.
25. Shi X, Kang Y, Hu Q, et al. A long-term observation of olfactory ensheathing cells transplantation to repair white matter and functional recovery in a focal ischemia model in rat. *Brain Res* 2010;1317:257–67.
26. Basso DM, Beattie MS, Bresnahan JC. Graded histological and locomotor outcomes after spinal cord contusion using the NYU weight-drop device versus transection. *Exp Neurol* 1996;139: 244–56.
27. Dubreuil CI, Winton MJ, McKerracher L. Rho activation patterns after spinal cord injury and the role of activated Rho in apoptosis in the central nervous system. *J Cell Biol* 2003;162:233–43.
28. Dusart I, Schwab ME. Secondary cell death and the inflammatory reaction after dorsal hemisection of the rat spinal cord. *Eur J Neurosci* 1994;6:712–24.
29. Hayashi M, Ueyama T, Nemoto K, et al. Sequential mRNA expression for immediate early genes, cytokines, and neurotrophins in spinal cord injury. *J Neurotrauma* 2000;17:203–18.
30. Pineau I, Lacroix S. Proinflammatory cytokine synthesis in the injured mouse spinal cord: multiphasic expression pattern and identification of the cell types involved. *J Comp Neurol* 2007;500: 267–85.
31. Nakamura M, Houghtling RA, MacArthur L, et al. Differences in cytokine gene expression profile between acute and secondary injury in adult rat spinal cord. *Exp Neurol* 2003;184:313–25.
32. Tartaglia LA, Ayres TM, Wong GH, et al. A novel domain within the 55 kd TNF receptor signals cell death. *Cell* 1993;74:845–53.
33. Lee YB, Yune TY, Baik SY, et al. Role of tumor necrosis factor-alpha in neuronal and glial apoptosis after spinal cord injury. *Exp Neurol* 2000;166:190–5.
34. Yune TY, Chang MJ, Kim SJ, et al. Increased production of tumor necrosis factor-alpha induces apoptosis after traumatic spinal cord injury in rats. *J Neurotrauma* 2003;20:207–19.
35. Deng Y, Lu J, Sivakumar V, et al. Amoeboid microglia in the periventricular white matter induce oligodendrocyte damage through expression of proinflammatory cytokines via MAP kinase signaling pathway in hypoxic neonatal rats. *Brain Pathol* 2008;18:387–400.
36. Shuman SL, Bresnahan JC, Beattie MS. Apoptosis of microglia and oligodendrocytes after spinal cord contusion in rats. *J Neurosci Res* 1997;50:798–808.
37. Zhang SC, Goetz BD, Carré JL, et al. Reactive microglia in dysmyelination and demyelination. *Glia* 2001;34:101–9.
38. Mohler KM, Torrance DS, Smith CA, et al. Soluble tumor necrosis factor (TNF) receptors are effective therapeutic agents in lethal endotoxemia and function simultaneously as both TNF carriers and TNF antagonists. *J Immunol* 1993;151:1548–61.
39. Spencer-Green G. Etanercept (Enbrel): update on therapeutic use. *Ann Rheum Dis* 2000;59(Suppl 1):146–9.
40. Springer JE, Azbill RD, Knapp PE. Activation of the caspase-3 apoptotic cascade in traumatic spinal cord injury. *Nat Med* 1999;5:943–6.
41. Casha S, Yu WR, Fehlings MG. Oligodendroglial apoptosis occurs along degenerating axons and is associated with FAS and p75 expression following spinal cord injury in the rat. *Neuroscience* 2001;103:203–18.
42. Ashkenazi A, Dixit VM. Death receptors: signaling and modulation. *Sci* 1998;281:1305–8.
43. Hisahara S, Shoji S, Okano H, et al. ICE/CED-3 family executes oligodendrocyte apoptosis by tumor necrosis factor. *J Neurochem* 1997;69:10–20.
44. Gupta S. A decision between life and death during TNF-alpha-induced signaling. *J Clin Immunol* 2002;22:185–94.

Spine

SPINE Volume 36, Number 25, pp 2122–2129

BASIC SCIENCE

High-Mobility Group Box-1 and Its Receptors Contribute to Proinflammatory Response in the Acute Phase of Spinal Cord Injury in Rats

Ke-Bing Chen, MD,*† Kenzo Uchida, MD, PhD,* Hideaki Nakajima, MD, PhD*, Takafumi Yayama, MD, PhD,* Takayuki Hirai, MD,* Alexander Rodriguez Guerrero, MD,*‡ Shigeru Kobayashi, MD, PhD,* Wei-Ying Ma, MD,*†§ Shao-Yu Liu, MD, PhD,† Ping Zhu, MD, PhD,*‖ and Hisatoshi Baba, MD, PhD*

Study Design. To examine the localization and expression of high-mobility group box-1 (HMGB-1) protein and its receptors after rat spinal cord injury.

Objective. To elucidate the contribution of HMGB-1 and its receptors as potential candidates in a specific upstream pathway to the proinflammatory response leading to a cascade of secondary tissue damage after spinal cord injury.

Summary of Background Data. HMGB-1 was recently characterized as a key cytokine with a potential role in nucleosome formation and regulation of gene transcription. No studies have investigated the role of HMGB-1 in spinal cord injury.

Methods. Injured thoracic spinal cord from 62 rats aged 8 to 12 weeks and spinal cord from 20 control rats were examined. HMGB-1 was localized by immunofluorescence staining, costaining with cell markers, and by immunoelectron microscopy. The expression of HMGB-1 and its receptors, receptor for advanced glycation end products (RAGE), toll-like receptor (TLR)2, and TLR4 were also examined by immunohistochemistry.

Results. HMGB-1 expression appeared earlier than that of tumor necrosis factor-α, interleukin *(IL)-1β*, and *IL-6* in the spinal cord injury rats, with the HMGB-1 produced by both macrophages and neurons. HMGB-1 translocated from nucleus to cytoplasm in some neurons at an early stage after neural injury. Increased expression of HMGB-1, RAGE, and TLRs was observed after injury, and interaction of HMGB-1 with RAGE or TLRs, particularly in macrophage, was confirmed at 3 days after injury.

Conclusion. Our results demonstrated an earlier onset in the expression of HMGB-1 than in tumor necrosis factor-α, *IL-1β*, and *IL-6* after spinal cord injury. The release of HMGB-1 from neurons and macrophages is mediated through the HMGB-1/RAGE or TLR pathways. HMGB-1 seems to play at least some roles in the proinflammatory cascade originating the secondary damage after the initial spinal cord injury.

Key words: high-mobility group box-1 (HMGB-1), proinflammatory cytokine, receptor for advanced glycation end products (RAGE), spinal cord injury, toll-like receptor (TLR). **Spine 2011;36:2122–2129**

Traumatic injury of the spinal cord initiates a cascade of secondary tissue damage beyond the original site of trauma, leading to a further loss of tissue and function.[1–3] The cascade of secondary tissue damage is accompanied by an inflammatory response marked by infiltration of neutrophils and macrophages, activation of glial cells, and upregulated expression of proinflammatory cytokines.[4–6] All these responses will lead to increased vascular permeability, edema, and degradation of the extracellular matrix. Proinflammatory cytokines, including tumor necrosis factor *(TNF)-α*, interleukin *(IL)-1β*, and *IL-6* are upregulated early in the inflammatory response. Such cytokines are involved in the regulation of leukocyte recruitment and activation of macrophages as well as microglia.[7] The importance of the inflammatory response in the pathophysiology of spinal cord injury is well recognized. However, while proinflammatory cytokines have cytotoxic effects on the nervous system, they also induce neurotrophic molecules to repair the injured tissue, although the precise effects and functions of these molecules remain controversial.[8–11] Besides, the initial mechanisms related to the injury event and its mediators remain speculative; while most of those, for example, the cellular materials and DNA released from damaged cells, are not considered specific.

The high-mobility group box-1 (HMGB-1) is a 216-amino acids (29-kDa) DNA-binding protein with a highly conserved

From the *Department of Orthopaedics and Rehabilitation Medicine, Faculty of Medical Sciences, The University of Fukui, Fukui, Japan; †Department of Spine Surgery, The First Affiliated Hospital, Sun Yat-Sen University, Guangzhou, People's Republic of China; ‡Servicio de Neurocirugia, Hospital Nacional Rosales, Universidad de El Salvador, San Salvador, El Salvador; §Department of Anaesthesiology, The Second Affiliated Hospital, Sun Yat-Sen University, Guangzhou, People's Republic of China; and ‖Guangdong General Hospital, Guangdong Academy of Medical Science, Guangzhou, People's Republic of China.

Acknowledgment date: April 1, 2010; Revision date: October 19, 2010; Acceptance date: October 23, 2010.

The manuscript submitted does not contain information about medical device(s)/drug(s).

Grant funds were received in support of this work. No benefits in any form have been or will be received from a commercial party related directly or indirectly to the subject of this manuscript.

Address correspondence and reprint requests to Kenzo Uchida, MD, PhD, Department of Orthopaedics and Rehabilitation Medicine, Faculty of Medical Sciences, The University of Fukui, Matsuoka Shimoaizuki 23-3, Eiheiji, Fukui 910-1193, Japan; E-mail: kuchida@u-fukui.ac.jp

DOI: 10.1097/BRS.0b013e318203941c

structure expressed in several species.[12] It is a ubiquitous and abundant nuclear protein known to participate in nucleosome formation and regulation of gene transcription.[13,14] HMGB-1 was recently characterized as a key cytokine[15,16] that induces a delayed and biphasic release of TNF distinct from that seen with endotoxin activation.[17] HMGB-1 is released from necrotic and inflammatory cells and induces an inflammatory response.[18] Furthermore, extracellular HMGB-1 is a potent proinflammatory molecule that induces TNF-α and IL-1β synthesis and secretion in monocyte and/or macrophages.[19] However, the role of HMGB-1 as a proinflammatory cytokine after spinal cord injury has not been studied in detail.

The local concentration of extracellular HMGB-1 can rapidly increase in the central nervous system through active exportation from the nucleus or as a consequence of passive cell leakage. Several cells of the central nervous system actively export HMGB-1 when exposed to appropriate stimuli,[20,21] and a massive accumulation of HMGB-1 outside necrotic cells occurs immediately after cerebral ischemic injury.[21] Once released, HMGB-1 binds with several surface molecules, including the receptor for advanced glycation end products (RAGE), toll-like receptor (TLR)2, and TLR4. RAGE belongs to the immunoglobulin superfamily[22,23] and is expressed in neurons, glias, and endothelial cells in the brain.[24] Activation of macrophages *via* TLRs is important for inflammation and host defense against pathogens.[25] In addition, recent data suggest that nonpathogenic molecules released by trauma in the central nervous system can also trigger inflammation *via* TLR2 and TLR4.[26,27]

In this study, we focused on the importance of HMGB-1 as a potential candidate in a specific upstream pathway that promotes inflammation after spinal cord injury. We hypothesize that HMGB-1 is likely to be an upstream inflammatory cytokine involved in the regulation of *TNF-α*, *IL-1β*, and *IL-6* secretion. Therefore, the localization and expression of HMGB-1 were examined in the acute phase after spinal cord injury by using immunohistochemical analysis. This is the first reported analysis of proinflammatory activation mediated through the HMGB-1/RAGE or TLR pathways in spinal cord injury.

MATERIALS AND METHODS

Animal Model of Spinal Cord Injury

The study was carried out at the Orthopaedic Spinal Cord Laboratory of Fukui University, Japan. The experimental protocol strictly followed the ethics review committee guidelines for animal experimentation of our university. Experiments were conducted in 82 adult male Sprague-Dawley rats (Clea, Tokyo, Japan), aged 8 to 10 weeks with a mean body weight of 272 ± 30.2 g (mean ± SD). After anesthesia by intraperitoneal injection of sodium pentobarbiturate (0.05 mg/g body weight), laminectomy was performed at the T9 and T10 levels by using a surgical microscope (VANOX-S, Olympus, Tokyo, Japan), taking utmost care in avoiding lesion to the dura mater. At the T10 segmental level, the dorsal surface of the spinal cord (n = 62) was compressed extradurally by using a 90-g static load (custom-made rod, 2 × 3 mm in diameter) for 2 minutes using the method described previously.[28,29] Rats subjected to laminectomy, but not spinal cord injury, comprised the control group (n = 20). After surgery, animals were housed under a 12-hour light-dark cycle in a bacteria-free, biologically clean room with access to food and water *ad libitum*.

Immunofluorescence Staining and Double Staining

At 2 hours, 6 hours, 12 hours, 1 day, 3 days, 1 week, and 2 weeks after injury, animals were reanesthetized, and 300 mL of phosphate-buffered saline (PBS) was perfused intracardially followed by perfusion of 200 mL of 2% paraformaldehyde in 0.1 M PBS (pH 7.6). Immediately after perfusion, the spinal cord segment from T8 to T12 was removed *en bloc* and stored in 0.1 M PBS containing 20% sucrose at 4°C for 36 hours. Tissue blocks were embedded in Tissue-Tek (optimal cutting temperature compound 4583, Sakura Finetechnical, Tokyo, Japan), frozen, and then stored at −80°C. Three control rats that underwent laminectomy without compression were also killed and processed as described previously.

Using a cryostat, serial 25-μm-thick transverse and sagittal frozen sections were prepared for immunofluorescence staining. All sections were serially mounted on glass slides and fixed with 2% paraformaldehyde in 0.1 M PBS for 5 minutes, sequentially rinsed in PBS, and then stored at −20°C. Serial 25-μm-thick transverse and sagittal frozen sections were also treated with 0.1M Tris-HCl buffer (pH 7.6) containing 0.3% Triton X-100 for another 24 hours to allow reaction of the cell membrane with the antibodies. Sections were incubated at 4°C overnight with primary monoclonal anti-HMGB-1 antibody (Ab79823, 1:100, rabbit IgG, Abcam plc, Cambridge, United Kingdom) diluted in Antibody Diluent with Background Reducing Components (Dako Cytomation, Carpenteria, CA). The secondary antibody was goat antirabbit Alexa Flour 488 conjugated antibody (1:250; Molecular Probes, Eugene, OR) applied for 1 hour at room temperature.

For immunofluorescence double staining, the sections were further incubated with antineuronal nuclei monoclonal antibody (MAb312RX, NeuN, 1:100, mouse IgG; Chemicon International, Temecula, CA), antimacrophage monoclonal antibody (Ab1211, OX-42, 1:100, CD11b, Abcam plc), antiglial fibrillary acidic protein monoclonal antibody (MAb3402X, GFAP 1:100, mouse IgG; Chemicon International) for astrocytes, anti-RAGE polyclonal antibody (SC8299, 1:100, goat IgG, Santa Cruz Biotechnology, Santa Cruz, CA), anti-TLR2 polyclonal antibody (SC16237, 1:100, goat IgG, Santa Cruz Biotechnology), or anti-TLR4 polyclonal antibody (SC16240, 1:100, goat IgG, Santa Cruz Biotechnology) diluted in Antibody Diluent with Background Reducing Components (Dako Cytomation) at 4°C overnight. The sections were then incubated with goat antimouse Alexa Flour 568 conjugated antibody (1:250; Molecular Probes). The immunostained cells were visualized under a fluorescent microscope (Olympus AX80) or confocal microscope equipped with a 15-mW krypton argon laser (model TCS SP2, Leica Instruments, Nussloch, Germany). The 488- and

568-nm lines of the argon/helium-neon laser were used for fluorescence excitation.

Immunoblot Analysis

Immunoblot analysis was performed at 2 hours, 6 hours, 12 hours, 1 day, 3 days, 1 week, and 2 weeks after spinal cord injury, using the method we described previously.[30,31] Immediately after anesthesia by intraperitoneal injection of sodium pentobarbiturate, the damaged spinal cord around the epicenter of the lesion (~20-mm long sections) was dissected *en bloc* from the spine and stored immediately at −80°C in liquid nitrogen. Sections were centrifuged at 15,000 × g for 30 seconds by using a BioMasher Rapid Homogenization Kit (Funakoshi, Tokyo, Japan). The samples were then solubilized in RIPA buffer (50 mM Tris-HCl, pH 7.5, 150 mM NaCl, 1% Triton X-100, 0.5% sodium deoxycholate, 20 μg/mL leupeptin, and 1 mM phenylmethylsulfonylfluoride), homogenized, and then stored at −80°C. Protein concentration was determined by a DC Protein Assay Kit (Bio-Rad Laboratories, Hercules, CA). Laemmli sodium dodecylsulfate buffer samples containing proteins were boiled and subjected to immunoblot analysis. Total protein (20 μg per lane) was separated on 12.5% sodium dodecyl sulfate polyacrylamide gel electrophoresis and transferred onto polyvinylidene difluoride membrane (PE Applied Biosystems, Foster, CA) for 70 minutes using a semidry blot apparatus. The membrane was washed twice in tris-buffered saline containing 0.05% Tween 20, blocked by 5% skim milk in PBS for 1 hour at room temperature, and then incubated with either polyclonal anti-HMGB-1 antibody (Ab18256, 1:1000, rabbit IgG, Abcam plc), anti-*TNF-α* (Ab9755, 1:500, rabbit IgG, Abcam plc), anti-*IL-1β* (Ab9787, 1:500, rabbit IgG, Abcam plc), anti-*IL-6* (SC1265, 1:1000, mouse IgG, Abcam plc), anti-RAGE (SC8299, 1:500, goat IgG, Santa Cruz Biotechnology), anti-TLR2 (SC16237, 1:500, goat IgG, Santa Cruz Biotechnology), or anti-TLR4 (SC16240, 1:500, goat IgG, Santa Cruz Biotechnology) overnight at 4°C, followed sequentially by antirabbit or antimouse IgG antibody and avidin-biotinylated peroxidase complex (1:10000; Envision System-HRP Labeled Polymer, Dako Cytomation) for 30 minutes each. After triple washing in 0.1M PBS, the membrane was incubated in enhanced chemiluminescence reagent for 1 minute and then the antibody binding was visualized by using a FluorChem 8000 System (Alpha Innotech Corporation, San Leandro, CA). The amount of each band of HMGB-1, *TNF-α*, *IL-1β* and *IL-6* was normalized to β-actin (IMG-5142A, 1:1000, rabbit IgG, Imgenex, San Diego, CA) as a semiquantitative data.

Immunohistochemistry for Electron Microscopy

At 0, 2, and 6 hours after injury, animals were perfused with the same perfusion fixative, as described previously, for immunohistochemistry but with the addition of 0.1% glutaraldehyde. Serial 25-μm-thick transverse frozen sections mounted on glass slides were treated with 0.1 M PBS containing 0.1 M glycine at room temperature for 30 minutes. For immunohistochemical staining, the sections were incubated at 4°C with polyclonal anti-HMGB-1 antibody (Ab79823, 1:100, rabbit IgG, Abcam plc) diluted in PBS at 4°C overnight. Slides were then washed in PBS three times for 5 minutes each, and sections were further incubated for 30 minutes with diluted biotinylated secondary antibody solution followed by washing for 5 minutes in PBS. The sections were again incubated for 30 minutes with VECTASTAIN ABC Reagent (Vectastain Elite Kit, Vector Laboratories, Burlingame, CA) and washed for 5 minutes in PBS. Finally, the sections were stained with 3,3-diaminobenzidine tetrahydrochloride (Dojin Chemicals, Tokyo, Japan) in PBS (pH 7.4) containing 0.01% H_2O_2 solution until the development of the desired staining intensity, rinsed in PBS, dehydrated using a graded series of ethanol, cleared in xylene, and flat-mounted in Spurr's resin on glass slides. After curing, the sections were examined, and areas of interests were cut out and glued to Spurr cylinders for ultrathin sectioning. The ultrathin sections were stained with uranyl acetate and lead citrate and examined on a Hitachi H-7650 transmission electron microscope (Hitachi, Tokyo, Japan).

Statistical Analysis

All values are expressed as mean ± SD. Differences between groups were examined for statistical significance using the paired *t* test. A *P* value less than 0.05 denoted the presence of a significant difference between groups. The previous tests were conducted by using SPSS software version 11.0 (SPSS Inc., Chicago, IL).

RESULTS

Temporal Pattern of Inflammatory Cytokine Expression

Differences in expression among HMGB-1, *TNF-α*, *IL-1β*, and *IL-6* in spinal cord were assessed by immunoblot analysis (Figure 1), with each cytokine in the injured spinal cord region assayed at several time points after spinal cord injury. The expression of HMGB-1 was significantly upregulated from 6 hours to 1 week after injury compared with control rats. The expressions of *TNF-α* and *IL-1β* were significantly upregulated at 1 and 3 days, while that of *IL-6* was higher from 3 days to 2 weeks after spinal cord injury compared with controls. HMGB-1 expression thus increased at an earlier phase after injury than the other cytokines.

Cellular Localization of HMGB-1 After Spinal Cord Injury

The immunofluorescent-stained sections were evaluated for the distribution of HMGB-1-positive cells in the injured spinal cord and detection of the sources and time course of HMGB-1 expression. Figure 2 indicates the time-course distribution of HMGB-1-positive cells in the 10 mm of tissue rostral and caudal to the injured epicenter. At 6 hours after spinal cord injury, HMGB-1-positive cells were present mainly around the injured site in the posterior funiculus. In addition, there were some positive cells in white matter, and also in the anterior horn (Figure 2A). The expression of HMGB-1 reached a peak level at 3 days after injury, when many positive cells were observed in both gray and white matter on axial and

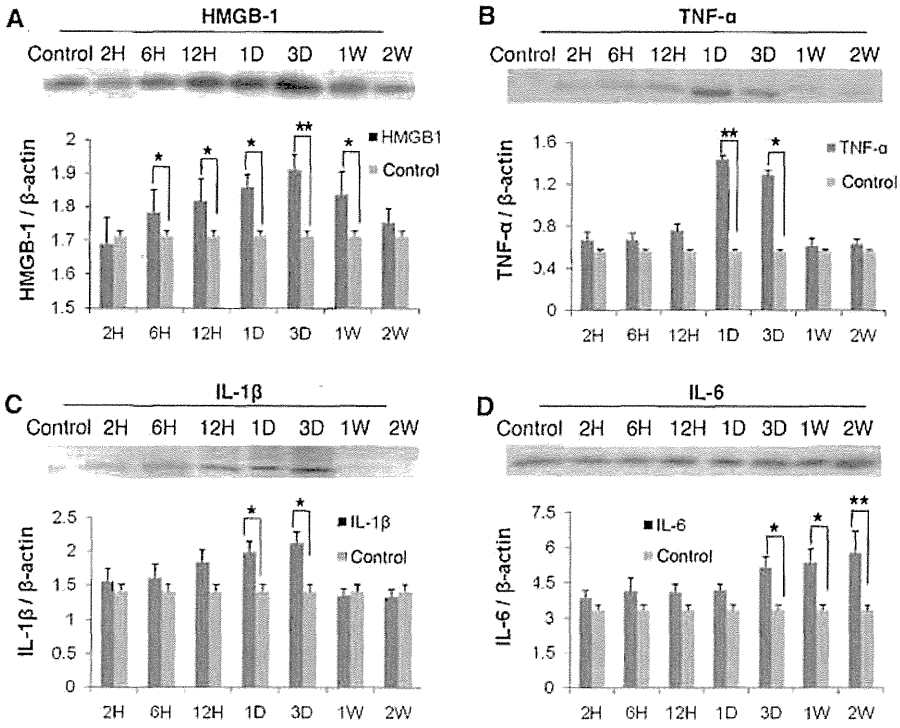

Figure 1. Immunoblot analysis showing the expression of high-mobility group box-1 (HMGB-1) (A), tumor necrosis factor *(TNF)-α* (B), interleukin *(IL)-1β* (C), and *IL-6* (D). Graphs indicate relative expression of bands compared with that of β-actin. The intensity of the band in injured spinal cord (n = 3 for each time point) was significantly high at 6 hours, 12 hours, 1 day, and 3 days in HMGB-1 (A), at 1 and 3 days in *TNF-α* (B) and *IL-1β* (C), and at 3 days, 1 week, and 2 weeks in *IL-6* (D), compared with that in control animals (n = 2 for each time point). H indicates hour; D, day; W, week. Data are expressed as mean ± SD. $^{*}P < 0.05$, $^{\dagger}P < 0.01$, compared to the density of β-actin.

transverses sections (Figure 2B, E). The number of positive cells gradually decreased, and some positive cells were still present in the gray and white matters at 2 weeks after spinal cord injury (Figure 2C). Control rats at 3 days after spinal cord injury showed a few, weakly immunoreactive HMGB-1-positive cells in the gray matter (Figure 2D).

To further evaluate the cellular location of HMGB-1 expression, double immunofluorescent staining with combinations of antibodies was performed, namely HMGB-1/NeuN (for neurons), HMGB-1/OX-42 (for macrophages), and HMGB-1/GFAP (for astrocytes). The results (Figure 3) showed that spinal cord injury-induced HMGB-1 expression was mostly localized in neurons in the gray matter and macrophages in the white matter but not in astrocytes.

At the electron microscope level, very scarce HMGB-1 expression was evident within the anterior horn cells at 0 hour (Figure 4A). At 2 hours after injury, the nuclear expression of HMGB-1 was markedly increased (Figure 4B), while at 6 hours after spinal cord injury, expression was detected in the cytoplasm (Figure 4C). These findings indicate that HMGB-1 is primarily localized in the nucleus of neurons early after spinal cord injury and that translocation to the cytoplasm occurs after a few hours with the increased expression.

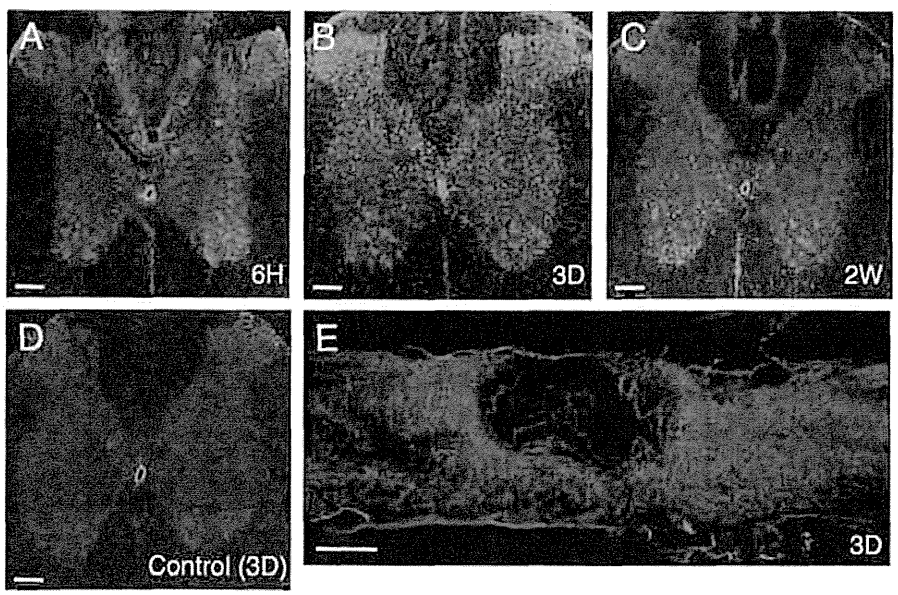

Figure 2. Photomicrographs showing distribution of high-mobility group box-1 (HMGB-1)-positive cells at 6 hours (A), 3 days (B), and 2 weeks (C) after spinal cord injury, and 3 days in control animals (D) in transverse sections at the injury level and 3 days after spinal cord injury in sagittal sections (E) (n = 3 for transverse sections and n = 2 for sagittal sections from each time point). Control rats showed few HMGB-1-positive cells in the gray matter (n = 3). At 6 hours after injury, HMGB-1-positive cells were mainly observed around the injured site in the posterior funiculus and in the anterior horn. Expression of HMGB-1 peaked at 3 days after injury, with immunopositive cells distributed throughout the gray and white matters. At 2 weeks after injury, the expression of HMGB-1 was low. Scale bar = 100 μm (A–D), 1 mm (E).

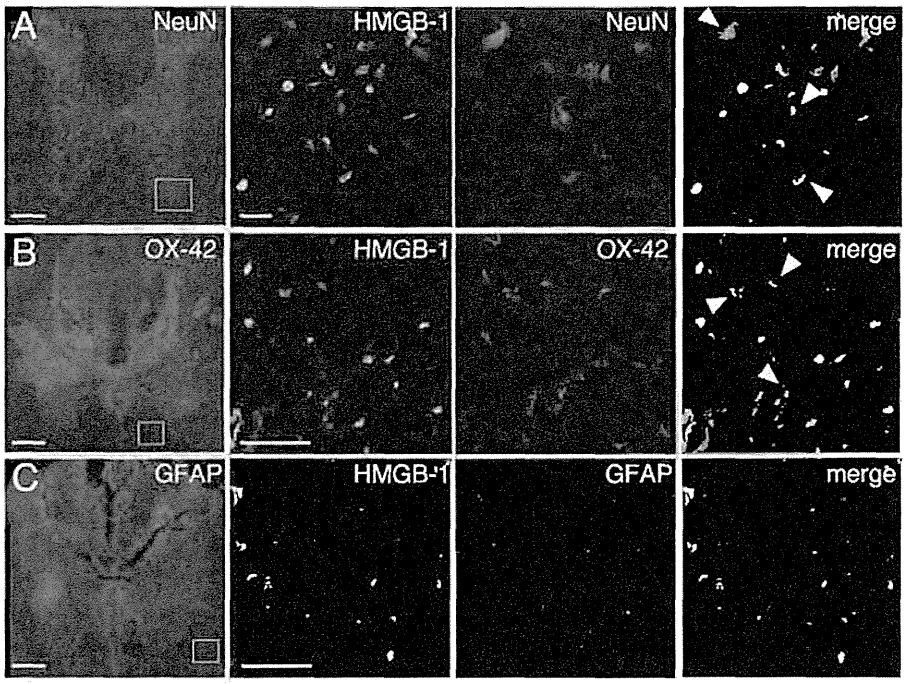

Figure 3. Photomicrograph showing the colocalization of cell-specific markers (red) and high-mobility group box-1 (HMGB-1) (green) in the injured spinal cord at 3 days after injury (n = 3). The box area in the left row indicates the location of high-magnification photomicrographs. Expression of HMGB-1 was significant in neurons (NeuN) (A) and microglia (OX-42) (B), which can best be appreciated in the merged images (yellow: arrowhead), but no expression was seen in the astroglia (GFAP) (C). Arrowheads indicated colocalization of HMGB-1 and the cell-specific marker. Scale bar = 100 μm (left column), 50 μm (HMGB-1 photomicrographs).

Interaction of HMGB-1 With RAGE, TLR2, and TLR4

Next, immunoblot analysis was performed at several time points after spinal cord injury to assess the postinjury expression of cell-surface proteins RAGE, TLR2, and TLR4. The results (Figure 5) showed a similar temporal expression pattern for RAGE to that of HMGB-1 after spinal cord injury, with RAGE significantly upregulated from 12 hours to 3 days after spinal cord injury compared with the levels in control rats. TLR2 and TLR4 remained at baseline levels 1 day after injury, but they were upregulated at 3 days.

To explore the interaction of extracellular HMGB-1 with these receptor molecules, double immunofluorescent staining, using combinations of antibodies, was performed. Colocalization of HMGB-1 and each receptor was clearly observed in the white matter (Figure 6). These results indicate that extracellular spinal cord injury-induced HMGB-1 functions mainly in activated microglia/macrophages.

DISCUSSION

This study characterized the localization and expression of HMGB-1 and its receptors in a rat spinal cord injury model and determined the role of HMGB-1 as an upstream cytokine within a cascade of secondary tissue damage after spinal cord injury. The main findings of our study were as follows: (1) appearance of HMGB-1 expression earlier than that of *TNF-α*, *IL-1β*, and *IL-6* in the spinal cord, with the source of HMGB-1 not only activated macrophages but also neurons. Related to this finding, HMGB-1 was translocated from the nucleus to the cytoplasm of neurons at an early stage after spinal cord injury; (2) the peak expression of HMGB-1 and its receptors RAGE, TLR2, and TLR4 in macrophages appeared simultaneously around 3 days after injury. Together, these results implicate HMGB-1 as the likely upstream cytokine that regulates the release of *TNF-α*, *IL-1β*, and *IL-6* after spinal cord injury. In addition, this secretion of HMGB-1 by neurons and macrophages, which is mediated through the HMGB-1/RAGE or TLR pathways, could participate in the proinflammatory cascade of secondary damage after spinal cord injury.

HMGB-1 seems to have two distinct functions in cellular systems. It functions as an intracellular regulator of transcription, and, in an extracellular role, it promotes tumor metastasis and inflammation.[32–34] Extracellular HMGB-1 participates in inflammatory processes that can lead to tissue damage and even death, including delayed endotoxin lethality and acute lung injury.[35,36] Monocytes and macrophages stimulated

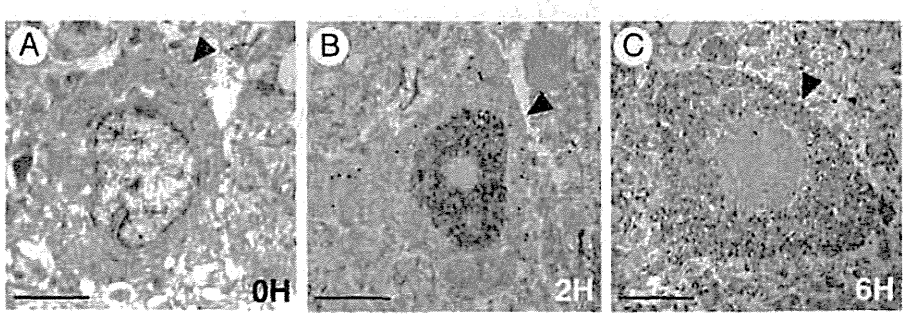

Figure 4. Immunoelectron microscopy demonstrated high-mobility group box-1 (HMGB-1) expression in the anterior horn cells (arrowheads) at 0 hour (A), 2 hours (B), and 6 hours (C) after spinal cord injury (n = 3 for each time point). HMGB-1 expression was localized in the nucleus in the anterior horn cells at 2 hours, while at 6 hours after spinal cord injury expression was markedly observed in the cytoplasm, not the nucleus. Scale bar = 10 μm (A–C).

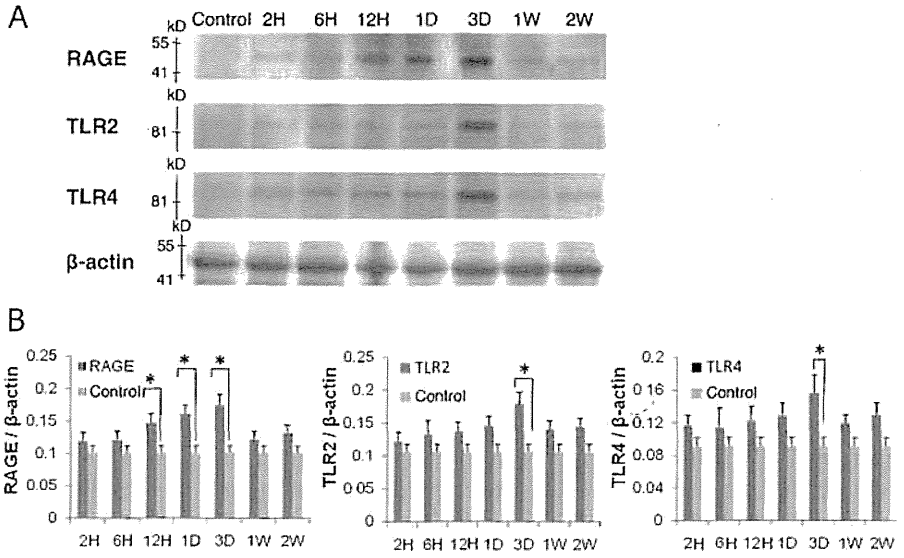

Figure 5. Immunoblot results showing expression of receptor for advanced glycation end products (RAGE), toll-like receptor (TLR)2, and TLR4 at several time intervals after spinal cord injury (A) (n = 3 for each time point). Graphs indicate relative expression of bands compared with the intensity of β-actin (B). The intensity of RAGE bands in injured spinal cord was significantly high from 12 hours after spinal cord injury compared to the comparable band in control rats (n = 2 for each time point). The protein expression gradually lessened from 1 week after spinal cord injury. The band intensities for TLR2 and TLR4 were significantly high at 3 days after injury. H indicates hour; D, day; W, week. Data are expressed as mean ± SD. $^*P < 0.05$, compared to the density of β-actin.

by lipopolysaccharide (LPS), *TNF-α*, or IL-1 secrete HMGB-1.[17,35] Indeed, monocytes cultured with HMGB-1 release *TNF-α*, IL-1, IL-1Ra, *IL-6, IL-8,* macrophage inflammatory protein-1, and macrophage inflammatory protein-1 but not anti-inflammatory cytokines, such as IL-10 and IL-12.[17,35] This production of proinflammatory cytokines after exposure to HMGB-1 occurs with delayed kinetics compared with the same response induced by LPS stimulation. For example, macrophages cultured with LPS secrete TNF-α within 1 hour, whereas TNF-α synthesis after HMGB-1 exposure begins only after 2 hours and persists up to 8 hours.[35,37] In the current study, HMGB-1 expression in the injured spinal cord appeared at an earlier phase than that of *TNF-α*, *IL-1β*, and *IL-6*. These results indicated that HMGB-1 could be an early trigger for proinflammatory activation after spinal cord injury, although multiple pathways, including macrophage activation and release of proinflammatory cytokines, probably play a role.

In this study, hematogenous inflammatory cells (neutrophils and macrophages) did not start to infiltrate the injured spinal cord until 6 to 12 hours postinjury and reached a peak at 24 hours (data not shown). These data suggest that these inflammatory cells are recruited by chemoattractants. Previous studies demonstrated that the rapid rise in *IL-1β*, *IL-6*, and *TNF-α* some hours after injury was followed by a dramatic decline before the peak appearance of neutrophils and macrophage.[38,39] Similar findings were noted in the present study in a rat spinal cord injury model; that is, the upregulation of cytokines was noted before the appearance of neutrophils and macrophages, suggesting that the spinal cord cells are the primary source of these inflammatory mediators rather than the later-arriving blood-born leukocytes.

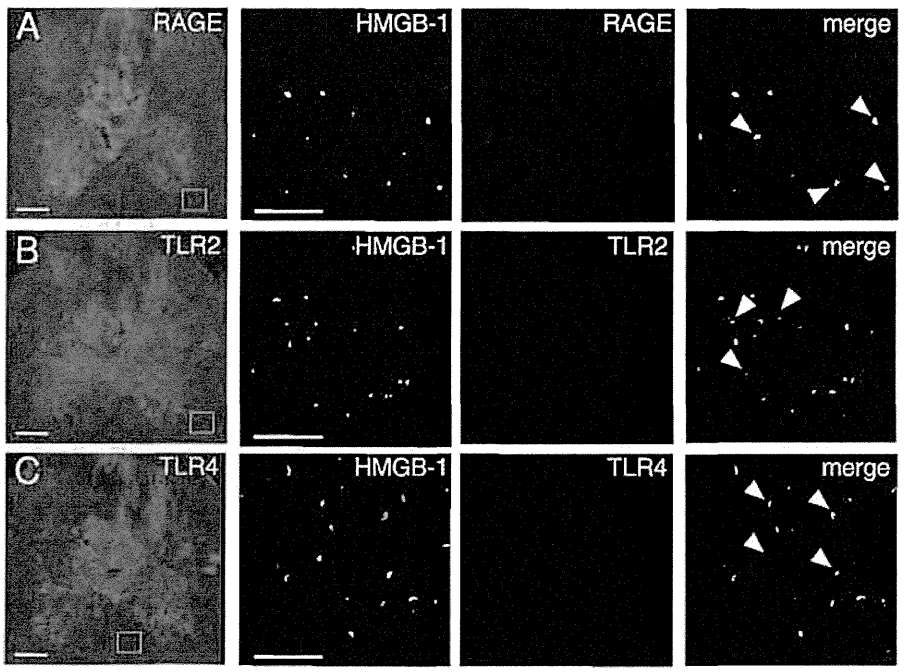

Figure 6. Photomicrograph showing the colocalization of receptor for advanced glycation end products (RAGE), toll-like receptor (TLR)2, and TLR4 (red) with high-mobility group box-1 (HMGB-1) (green) in injured spinal cord at 3 days after injury (n = 3). The expression of these receptors was observed in both gray and white matter. Colocalization of HMGB-1 and RAGE (A), TLR2 (B), or TLR4 (C) was observed in the white matter (yellow: arrowhead). The box area in the left row indicates high-magnification micrographs. Scale bar = 100 μm (left column) or 50 μm (HMGB-1 photomicrographs).

Previous studies showed that HMGB-1 can be released into the extracellular space either actively from macrophage and/or monocytes after HMGB-1 is hyperacetylated in the nucleus[40] or passively when HMGB-1 diffuses out of the damaged plasma membranes of necrotic cells.[33] Such cells that become deficient in HMGB-1 have diminished ability to induce inflammatory responses compared with wild-type cells.[33] Interestingly, apoptotic cells do not release significant quantities of HMGB-1, which is retained within the nuclear structure even when cell membrane integrity is lost. These cells therefore do not trigger the inflammation. These data can indicate that HMGB-1 is a critical stimulator of inflammation at the site of cell injury and death. The pathogenesis of spinal cord injury initially involves acute mechanical trauma, local deformation, and energy transformation at a very-early stage, resulting in cellular necrosis. Immunostaining in this study localized HMGB-1 in both macrophages and neurons, in particular, in the nucleus and cytoplasm of neurons. Recent studies demonstrated the release of HMGB-1 from neurons soon after brain ischemic injury[41] and HMGB-1 secreted from necrotic neural cells as the likely source of elevated serum HMGB-1.[42] It seems reasonable to suggest, therefore, that HMGB-1 can also be released by injured or necrotic neurons and subsequently participate as an early upstream initiator of inflammation after a traumatic injury to the spinal cord.

RAGE is a transmembrane protein and a member of the immunoglobulin superfamily. It is expressed in endothelial cells, vascular smooth muscle cells, neurons, and macrophages/monocytes.[43] As a receptor of multiple ligands, RAGE has also been implicated in mediating the cytokine activity of HMGB-1 in macrophages and tumor cells.[32,37,44] To our knowledge, RAGE overexpression in spinal cord injury has not yet been reported, although its role in β-amyloid metabolism, Alzheimer disease, and ischemic stroke has been studied.[41,45,46] RAGE signals through pathways that involve extracellular signal-regulated kinase (ERK)1 and ERK2, as well as the mitogen-activated protein kinase p38. It promotes the activation of nuclear factor (NF)-κB,[47] which itself activates the transcription of proinflammatory genes, such as *IL-1β*, *IL-6*, and *TNF-α*. On the contrary, the interaction of HMGB-1 with TLR2 and TLR4 also promotes inflammatory responses that ultimately lead to NF-κB activation and production of proinflammatory cytokines.[48] and damage of the central nervous system. TLRs are found predominantly on microglia and macrophages.[49] Recent data showed that TLRs initiate or propagate central nervous system pathology in models of autoimmune demyelination, cerebral ischemia, and peripheral neuropathy.[49–51]

In this study, RAGE expression increased in the earlier phases, coupled with increased TLR2 and TLR4 expression at a later phase, which is proportional to the activation process of macrophages. The interaction of HMGB-1 with RAGE, TLR2, and TLR4 were confirmed by our immunohistochemical analysis, particularly in macrophages. These results indicated that RAGE and some TLRs are important receptors in HMGB-1 intracellular signaling after spinal cord injury.

In conclusion, this study demonstrated earlier expression of HMGB-1 than *TNF-α*, *IL-1β*, and *IL-6* in the rat injured spinal cord and that the sources of HMGB-1 were both activated macrophages and neurons. The peak expression of HMGB-1 and RAGE appeared simultaneously, followed by TLR expression. Interactions were demonstrated between HMGB-1 and RAGE, TLR2, and TLR4 around 3 days after spinal cord injury. However, the major limitation of this study is that expressions of HMGB-1 and its receptors may be epiphenomena with expressions of *TNF-α*, *IL-1β*, and *IL-6*. Further studies are required to clarify the role of HMGB-1 and the possible beneficial effects of inhibition of HMGB-1 expression after spinal cord injury. Nevertheless, our findings suggest that HMGB-1, together with RAGE and the TLRs, seems to play at least some roles in cell damage or death, which in turn probably contributes to the initial inflammatory response generating the secondary damage of spinal cord injury.

➢ Key Points

- ❑ The increased expression of HMGB-1 in the acute phase of rat spinal cord injury exceeded that of *TNF-α*, *IL-1β*, and *IL-6*, with the HMGB-1 secreted not only from activated macrophages but also from neurons.
- ❑ HMGB-1 and its receptors, RAGE and TLRs, were expressed simultaneously around 3 days after spinal cord injury, particularly in macrophages.
- ❑ Our results suggested that HMGB-1, RAGE, and TLRs contribute to cell damage and/or death after spinal cord injury, probably during the initial inflammatory response that generates the secondary damage.

References

1. Blight AR. Macrophages and inflammatory damage in spinal cord injury. *J Neurotrauma* 1992;9(suppl 1):S83–91.
2. Bartholdi D, Schwab ME. Expression of pro-inflammatory cytokine and chemokine mRNA upon experimental spinal cord injury in mouse: an *in situ* hybridization study. *Eur J Neurosci* 1997;9:1422–38.
3. Ito T, Oyanagi K, Wakabayashi K, et al. Traumatic spinal cord injury: a neuropathological study on the longitudinal spreading of the lesions. *Acta Neuropathol* 1997;93:13–8.
4. Dusart I, Schwab ME. Secondary cell death and the inflammatory reaction after dorsal hemisection of the rat spinal cord. *Eur J Neurosci* 1994;6:712–24.
5. Hayashi M, Ueyama T, Nemoto K, et al. Sequential mRNA expression for immediate early genes, cytokines, and neurotrophins in spinal cord injury. *J Neurotrauma* 2000;17:203–18.
6. Pineau I, Lacroix S. Proinflammatory cytokine synthesis in the injured mouse spinal cord: multiphasic expression pattern and identification of the cell types involved. *J Comp Neurol* 2007;500:267–85.
7. Nakamura M, Houghtling RA, MacArthur L, et al. Differences in cytokine gene expression profile between acute and secondary injury in adult rat spinal cord. *Exp Neurol* 2003;184:313–25.
8. Rothwell NJ, Hopkins SJ. Cytokines and the nervous system II: actions and mechanisms of action. *Trends Neurosci* 1995;18:130–6.
9. Merrill JE, Benveniste EN. Cytokines in inflammatory brain lesions: helpful and harmful. *Trends Neurosci* 1996;19:331–8.

10. Bethea JR, Dietrich WD. Targeting the host inflammatory response in traumatic spinal cord injury. *Curr Opin Neurol* 2002;15: 355–60.
11. Inukai T, Uchida K, Nakajima H, et al. Tumor necrosis factor-alpha and its receptors contribute to apoptosis of oligodendrocytes in the spinal cord of spinal hyperostotic mouse (*twy/twy*) sustaining chronic mechanical compression. *Spine* 2009;34:2848–57.
12. Thomas JO. HMG1 and 2: architectural DNA-binding proteins. *Biochem Soc Trans* 2001;29:395–401.
13. Stros M, Ozaki T, Bacikova A, et al. HMGB1 and HMGB2 cell-specifically down-regulate the p53- and p73-dependent sequence-specific transactivation from the human Bax gene promoter. *J Biol Chem* 2002;277:7157–64.
14. Park JS, Svetkauskaite D, He Q, et al. Involvement of toll-like receptors 2 and 4 in cellular activation by high mobility group box 1 protein. *J Biol Chem* 2004;279:7370–7.
15. Lotze MT, Tracey KJ. High-mobility group box 1 protein (HMGB1): nuclear weapon in the immune arsenal. *Nat Rev Immunol* 2005;5:331–42.
16. Yang H, Wang H, Czura CJ, et al. The cytokine activity of HMGB1. *J Leukoc Biol* 2005;78:1–8.
17. Andersson U, Wang H, Palmblad K, et al. High mobility group 1 protein (HMG-1) stimulates proinflammatory cytokine synthesis in human monocytes. *J Exp Med* 2000;192:565–70.
18. Pisetsky DS, Erlandsson-Harris H, Andersson U. High-mobility group box protein 1 (HMGB1): an alarmin mediating the pathogenesis of rheumatic disease. *Arthritis Res Ther* 2008;10:209.
19. Chen G, Ward MF, Sama AE, et al. Extracellular HMGB1 as a proinflammatory cytokine. *J Interferon Cytokine Res* 2004;24: 329–33.
20. Wang H, Vishnubhakat JM, Bloom O, et al. Proinflammatory cytokines (tumor necrosis factor and interleukin 1) stimulate release of high mobility group protein-1 by pituicytes. *Surgery* 1999;126:389–92.
21. Kim JB, Sig Choi J, Yu YM, et al. HMGB1, a novel cytokine-like mediator linking acute neuronal death and delayed neuroinflammation in the postischemic brain. *J Neurosci* 2006;26:6413–21.
22. Brett J, Schmidt AM, Yan SD, et al. Survey of the distribution of a newly characterized receptor for advanced glycation end products in tissues. *Am J Pathol* 1993;143:1699–712.
23. Vincent AM, Perrone L, Sullivan KA, et al. Receptor for advanced glycation end products activation injures primary sensory neurons via oxidative stress. *Endocrinology* 2007;148:548–58.
24. Arancio O, Zhang HP, Chen X, et al. RAGE potentiates Abeta-induced perturbation of neuronal function in transgenic mice. *EMBO J* 2004;23:4096–105.
25. Anderson KV, Bokla L, Nüsslein-Volhard C. Establishment of dorsal-ventral polarity in the Drosophila embryo: the induction of polarity by the Toll gene product. *Cell* 1985;42:791–8.
26. Popovich PG. Immunological regulation of neuronal degeneration and regeneration in the injured spinal cord. *Prog Brain Res* 2000;128:43–58.
27. Kigerl KA, Lai W, Rivest S, et al. Toll-like receptor (TLR)-2 and TLR-4 regulate inflammation, gliosis, and myelin sparing after spinal cord injury. *J Neurochem* 2007;102:37–50.
28. Nakajima H, Uchida K, Kobayashi S, et al. Rescue of rat anterior horn neurons after spinal cord injury by retrograde transfection of adenovirus vector carrying brain-derived neurotrophic factor gene. *J Neurotrauma* 2007;24:703–12.
29. Nakajima H, Uchida K, Yayama T, et al. Targeted retrograde gene delivery of brain-derived neurotrophic factor suppresses apoptosis of neurons and oligodendroglias after spinal cord injury in rats. *Spine* 2010;35:497–504.
30. Uchida K, Baba H, Maezawa Y, et al. Increased expression of neurotrophins and their receptors in the mechanically compressed spinal cord of the spinal hyperostotic mouse (*twy/twy*). *Acta Neuropathol* 2003;106:29–36.
31. Uchida K, Nakajima H, Inukai T, et al. Adenovirus-mediated retrograde transfer of neurotrophin-3 enhances survival of anterior horn neurons of *twy/twy* mice with chronic mechanical compression of the spinal cord. *J Neurosci Res* 2008;86:1789–800.
32. Yang H, Wang H, Tracey KJ. HMG-1 rediscovered as a cytokine. *Shock* 2001;15:247–53.
33. Scaffidi P, Misteli T, Bianchi ME. Release of chromatin protein HMGB1 by necrotic cells triggers inflammation. *Nature* 2002;418:191–5.
34. Czura CJ, Tracey KJ. Targeting high mobility group box 1 as a late-acting mediator of inflammation. *Crit Care Med* 2003;31 (suppl 1):S46–50.
35. Wang H, Bloom O, Zhang M, et al. HMG-1 as a late mediator of endotoxin lethality in mice. *Science* 1999;285:248–51.
36. Abraham E, Arcaroli J, Carmody A, et al. HMG-1 as a mediator of acute lung inflammation. *J Immunol* 2000;165:2950–4.
37. Wang H, Yang H, Czura CJ, et al. HMGB1 as a late mediator of lethal systemic inflammation. *Am J Respir Crit Care Med* 2001;164:1768–73.
38. Dinarello CA. Interleukin-1. In: Thomson AW, ed. *The Cytokine Handbook*. 3rd ed. San Diego, CA: Academic Press, 1998:35–73.
39. Takao Y, Okajima K. Spinal cord injury in the rat. *Prog Neurobiol* 1998;56:341–58.
40. Bonaldi T, Talamo F, Scaffidi P, et al. Monocytic cells hyperacetylate chromatin protein HMGB1 to redirect it towards secretion. *EMBO J* 2003;22:5551–60.
41. Qiu J, Nishimura M, Wang Y, et al. Early release of HMGB-1 from neurons after the onset of brain ischemia. *J Cereb Blood Flow Metab* 2008;28:927–38.
42. Muhammad S, Barakat W, Stoyanov S, et al. The HMGB1 receptor RAGE mediates ischemic brain damage. *J Neurosci* 2008;28:12023–31.
43. Stern D, Yan SD, Yan SF, et al. Receptor for advanced glycation end products: a multiligand receptor magnifying cell stress in diverse pathologic settings. *Adv Drug Deliv Rev* 2002;54:1615–25.
44. Yang H, Wang H, Czura CJ, et al. HMGB1 as a cytokine and therapeutic target. *J Endotoxin Res* 2002;8:469–72.
45. Mackic JB, Stins M, McComb JG, et al. Human blood-brain barrier receptors for Alzheimer's amyloid-beta 1-40. Asymmetrical binding, endocytosis, and transcytosis at the apical side of brain microvascular endothelial cell monolayer. *J Clin Invest* 1998;102:734–43.
46. Deane R, Du Yan S, Submamaryan RK, et al. RAGE mediates amyloid-beta peptide transport across the blood-brain barrier and accumulation in brain. *Nat Med* 2003;9:907–13.
47. Park JS, Arcaroli J, Yum HK, et al. Activation of gene expression in human neutrophils by high mobility group box 1 protein. *Am J Physiol Cell Physiol* 2003;284:C870–9.
48. Ozinsky A, Underhill DM, Fontenot JD, et al. The repertoire for pattern recognition of pathogens by the innate immune system is defined by cooperation between toll-like receptors. *Proc Natl Acad Sci U S A* 2000;97:13766–71.
49. Zekki H, Feinstein DL, Rivest S. The clinical course of experimental autoimmune encephalomyelitis is associated with a profound and sustained transcriptional activation of the genes encoding toll-like receptor 2 and CD14 in the mouse CNS. *Brain Pathol* 2002;12:308–19.
50. Ma li ska D, Laure-Kamionowska M, Ma li ski S. Toll-like receptors in rat brains injured by hypoxic-ischaemia or exposed to staphylococcal alpha-toxin. *Folia Neuropathol* 2004;42:125–32.
51. Tanga FY, Nutile-McMenemy N, DeLeo JA. The CNS role of Toll-like receptor 4 in innate neuroimmunity and painful neuropathy. *Proc Natl Acad Sci U S A* 2005;102:5856–61.

J Neurosurg Spine 15:380–385, 2011

Outcomes of fusion surgery for ossification of the posterior longitudinal ligament of the thoracic spine: a multicenter retrospective survey

Clinical article

Morio Matsumoto, M.D.,[1] Yoshiaki Toyama, M.D.,[1] Hirotaka Chikuda, M.D.,[2] Katsushi Takeshita, M.D.,[2] Tsuyoshi Kato, M.D.,[3] Shigeo Shindo, M.D.,[4] Kuniyoshi Abumi, M.D.,[5] Masahiko Takahata, M.D.,[6] Yutaka Nohara, M.D.,[7] Hiroshi Taneichi, M.D.,[7] Katsuro Tomita, M.D.,[8] Norio Kawahara, M.D.,[8] Shiro Imagama, M.D.,[9] Yukihiro Matsuyama, M.D.,[10] Masashi Yamazaki, M.D.,[11] and Akihiko Okawa, M.D.[11]

[1]Department of Orthopedic Surgery, Keio University; [2]Department of Orthopaedic Surgery, Faculty of Medicine, University of Tokyo; [3]Department of Orthopaedic Surgery, Tokyo Medical and Dental University; [4]Department of Orthopaedic Surgery, Kudanzaka Hospital, Tokyo; Departments of [5]Spinal Reconstruction and [6]Orthopaedics, Hokkaido University Graduate School of Medicine, Sapporo; [7]Department of Orthopaedic Surgery, Dokkyo Medical University, Tochigi; [8]Department of Orthopaedic Surgery, School of Medicine, Kanazawa University, Kanazawa; [9]Department of Orthopaedic Surgery, Nagoya University Graduate School of Medicine, Nagoya; [10]Department of Orthopaedic Surgery, Hamamatsu University School of Medicine, Shizouka; and [11]Department of Orthopaedic Surgery, Chiba University Graduate School of Medicine, Chiba, Japan

Object. The aim of this study was to evaluate the outcomes of fusion surgery in patients with ossification of the posterior longitudinal ligament in the thoracic spine (T-OPLL) and to identify factors significantly related to surgical outcomes.

Methods. The study included 76 patients (34 men and 42 women with a mean age of 56.3 years) who underwent fusion surgery for T-OPLL at 7 spine centers during the 5-year period from 2003 to 2007. The authors evaluated the patient demographic data, underlying disease, preoperative comorbidities, history of spinal surgery, radiological findings, surgical methods, surgical outcomes, and complications. Surgical outcomes were assessed using the Japanese Orthopaedic Association (JOA) scale score for thoracic myelopathy (11 points) and the recovery rate.

Results. The mean JOA scale score was 4.6 ± 2.1 points preoperatively and 7.7 ± 2.5 points at the time of the final follow-up examination, yielding a mean recovery rate of 45.4% ± 39.1%. The recovery rates by surgical method were 38.5% ± 37.8% for posterior decompression and fusion, 65.0% ± 35.6% for anterior decompression and fusion via an anterior approach, 28.8% ± 41.2% for anterior decompression via a posterior approach, and 57.5% ± 41.1% for circumferential decompression and fusion. The recovery rate was significantly higher in patients without diabetes mellitus (DM) than in those with DM. One or more complications were experienced by 31 patients (40.8%), including 20 patients with postoperative neurological deterioration, 7 with dural tears, 5 with epidural hematomas, 4 with respiratory complications, and 10 with other complications.

Conclusions. The outcomes of fusion surgery for T-OPLL were favorable. The absence of DM correlated with better outcomes. However, a high rate of complications was associated with the fusion surgery.
(DOI: 10.3171/2011.6.SPINE10816)

Key Words • fusion • thoracic spine • ossification of the posterior longitudinal ligament

Ossification of the posterior longitudinal ligament in the thoracic spine (T-OPLL) is a rare but clinically significant spinal disorder that causes progressive thoracic myelopathy. Ohtsuka et al.[6] conducted a population-based survey in a rural area of Japan and reported a T-OPLL prevalence of 0.8%, which is significantly lower than the 3.2% prevalence of cervical OPLL. Therefore, a multicenter study to gather patient data for this rare disease is necessary to draw valid conclusions. A Research Group for Ossification of the Spinal Ligament, sponsored by the Japanese Ministry of Health, Labor and Welfare, conducted a multiinstitutional retrospective survey of 154 patients who underwent surgery for T-OPLL between 1998 and 2002.[4] That study identified significant

Abbreviations used in this paper: DM = diabetes mellitus; JOA = Japanese Orthopaedic Association; T-OPLL = ossification of the posterior longitudinal ligament in the thoracic spine.

factors related to surgical outcomes, which included T-OPLL in the upper thoracic spine, and the use of spinal instrumentation. The authors of that study and other earlier analyses indicated that decompression surgery alone, except laminoplasty, for T-OPLL in the lordotic upper thoracic spine often results in neurological deterioration after surgery, because decompression makes the thoracic spine unstable and therefore the spinal cord becomes more prone to compression by ventral T-OPLL.[4,10] While that study clarified that fusion surgery supplemented by spinal instrumentation was effective, it did not identify an optimal fusion method—anterior, posterior, or combined—for the best results and the fewest complications. Thus, we conducted a study of patients with T-OPLL who had undergone fusion surgery at 7 Japanese spine centers. The primary objective of this study was to determine the outcome of surgical treatment for T-OPLL by using the Japanese Orthopaedic Association (JOA) scale. The secondary objectives were to determine the patient, imaging, and surgical factors that influence outcomes and to determine the surgical complication rate and sequelae.

Methods

Approval for this study was obtained from the review boards of the participating institutions. Questionnaires were sent to each institution in November 2009 to collect data on consecutive patients who had undergone fusion surgery for T-OPLL during the 5-year period from 2003 to 2007 and who had been followed up for more than 1 year.

The data were collected by retrospective review of patient charts, databases, and radiological images at each participating institution. Initially, data for 82 patients were collected from all participating institutions; however, 6 patients were excluded from analysis because of a lack of detailed follow-up data. Thus, 76 patients, 34 men and 42 women, with a mean age of 56.3 years were ultimately included in the study (Table 1). The data collected for patients included demographics, the underlying disease, preoperative comorbidities, history of spinal surgery, radiological findings, surgical methods, outcomes, and complications.

Clinical Data

There were comorbid conditions in 45 patients (59.2%), including hypertension in 26 patients (34.2%) and diabetes mellitus (DM) in 19 (25%). Morphologically, T-OPLL was classified as the linear, beaked, continuous waveform, continuous cylindrical, or mixed type (composed of at least 2 of the first 4 types; Fig. 1).[4] Lateral view radiographs were used to determine the level of the ossified lesions. The T-OPLL was classified as beaked in 17 patients (22.4%), continuous waveform in 28 (36.8%), continuous cylindrical in 13 (17.1%), and mixed type in 18 (23.7%). None of the patients had the linear type of OPLL, although 6 patients had linear type OPLL combined with other OPLL types, and thus their disease was classified as the mixed type. The thoracic vertebral level at which maximum ossification occurred was determined using CT. Magnetic resonance imaging was utilized to determine the OPLL kyphosis angle and the presence or absence of an intramedullary high-intensity lesion on T2-weighted images.

TABLE 1: Summary of demographic data in 76 patients with T-OPLL

Characteristic	Value
sex	
M	34
F	42
mean age in yrs (range)	56.3 (26–82)
mean follow-up in yrs (range)	3.2 (1–6.5)
mean preop morbidity period (range)	1.9 yrs (1 mo–13 yrs 6 mos)

Surgical outcomes were assessed using the JOA scale score for thoracic myelopathy.[4] Recovery rates were calculated using the preoperative and follow-up examination JOA scale scores, according to the following formula: recovery rate = (JOA score at follow-up – preoperative JOA score)/(11 – preoperative JOA score) × 100(%). The JOA scale scores could be obtained in 66 patients (87%) at the 1-year follow-up and in 38 patients (50%) at the 3-year follow-up. The modified Frankel classification described by Bradford et al.[1] was used in addition to the JOA scale.

Statistical Analysis

For statistical analyses, we applied PASW Statistics (SPSS Japan, Inc.). A logistic regression analysis was conducted to find factors related to better surgical outcomes. A recovery rate of JOA scale scores 50% or higher was considered to be a good outcome as reported previously.[4] A p value < 0.05 was considered statistically significant.

Results

Radiological Data

The level of maximum ossification was the upper thoracic spine (T1–4) in 24 patients (31.6%), middle thoracic spine (T5–8) in 41 (53.9%), and lower thoracic spine (T9–12) in 11 (14.5%). The mean diameter of the ossified lesion measured at the largest level on CT scans was 7.8 ± 1.8 mm (range 3.0–11.0 mm). The mean kyphosis angle on MR images was 31.7° ± 9.5° (range 11°–58°), and a high-intensity lesion in the spinal cord was observed on the T2-weighted images in 59 patients (77.6%).

Surgical Methods

Posterior decompression and fusion was conducted in 47 patients (61.8%); anterior decompression and fusion via an anterior extra- or transpleural approach was performed in 12 (15.8%); anterior decompression via a posterior approach and posterior fusion (removal or floating of OPLL from the posterolateral sides of the spinal canal), as reported by Ohtsuka et al.[7,8] was performed in 4 (5.3%); and circumferential decompression and fusion via a combined anterior and posterior approach, as described by Tomita et al.,[9] was performed in 13 (17.1%; Fig. 2). No patient underwent a sternum-splitting approach in this

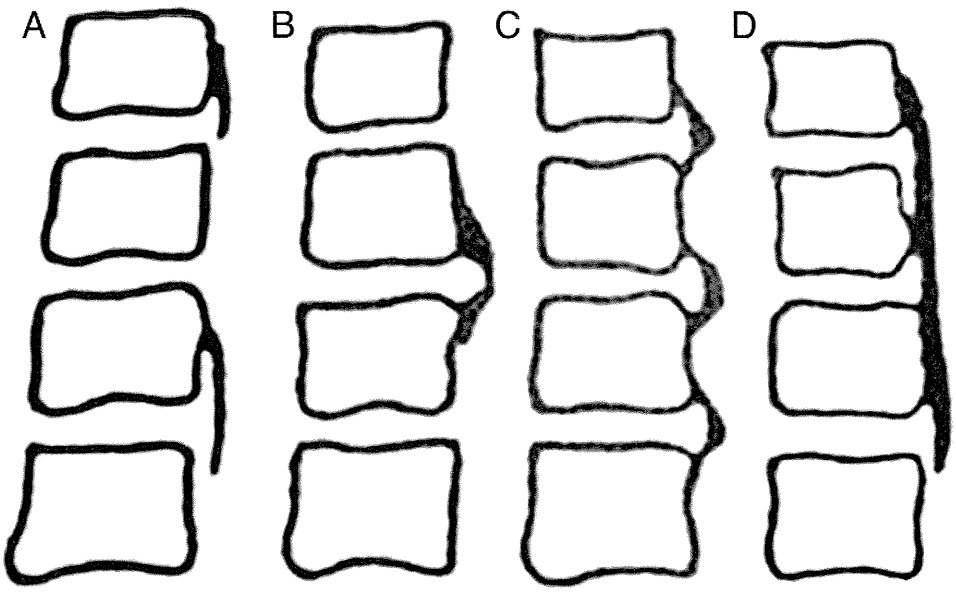

FIG. 1. Drawings depicting the T-OPLL classifications: linear **(A)**, beaked **(B)**, continuous waveform **(C)**, and continuous cylindrical **(D)**. The mixed type was defined as a combination of 2 or more types.

series. The choice of surgical method was not controlled in this study, but instead was determined according to the preference of each participating institution.

No differences were observed in the surgical method selected for the different T-OPLL morphological types or OPLL levels (Table 2). Spinal instrumentation was used in 69 patients (90.8%). Neurophysiological monitoring (isolated or combined use of somatosensory evoked potentials, motor evoked potentials, and spinal cord evoked potentials) was used in 58 patients (76.3%).

Surgical Outcomes

The mean JOA scale score was 4.6 ± 2.1 points preoperatively, 7.4 ± 2.4 points at 1 year postoperatively, 7.5 ± 2.4 points at 3 years postoperatively, and 7.7 ± 2.5 points at the final follow-up examination, yielding a mean recovery rate of 45.4% ± 39.1%. Thus, a statistically significant improvement in the JOA score was obtained at the time of the final follow-up examination ($p = 0.0001$, paired t-test). The recovery rate by surgical method was 38.5% ± 37.8% for posterior decompression and fusion, 65.0% ± 35.6% for anterior decompression and fusion via an anterior approach, 28.8% ± 41.2% for anterior decompression via a posterior approach, and 57.5% ± 41.1% for circumferential decompression and fusion.

Of the 73 patients whose modified Frankel grade was recorded both before and at the time of the follow-up examination, 60 patients (82.2%) improved by at least 1 grade, 9 (12.3%) remained unchanged, and 4 (5.5%) deteriorated by at least 1 grade.

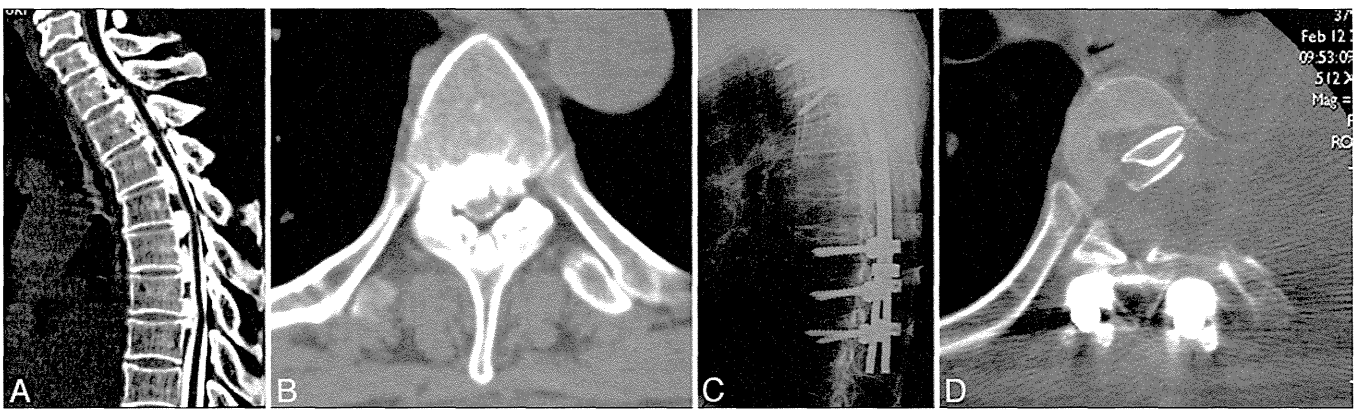

FIG. 2. Images obtained in a 49-year-old man with the continuous waveform type of OPLL. The patient was not ambulatory prior to surgery because of severe myelopathy. He underwent posterior decompression and fusion using spinal instrumentation. Since his neurological status remained almost the same as before surgery, he underwent anterior decompression and fusion via a transpleural approach 4 weeks after the posterior surgery. He had gradual neurological improvement and was able to resume walking with bilateral crutches 1 year after surgery. **A:** Sagittal reconstructed CT scan. **B:** Axial CT scan at the T-6 level. **C:** Lateral radiograph obtained after posterior decompression and fusion. **D:** A CT scan at the T-6 level obtained after anterior decompression and fusion.

TABLE 2: Surgical methods and type and level of OPLL*

Surgical Method	No.	Type of OPLL (no. [%])				Level of OPLL (no. [%])		
		Beaked	Continuous Waveform	Continuous Cylindrical	Mixed	T1–4	T5–8	T9–12
total	76	17 (22.4)	28 (36.8)	13 (17.1)	18 (23.7)	24 (31.6)	41 (53.9)	11 (14.5)
pst decompression & fusion	47	10 (58.8)	20 (71.4)	8 (61.5)	9 (50)	18 (75.0)	23 (56.1)	6 (54.5)
ant decompression & fusion via ant approach	12	4 (23.5)	3 (10.7)	1 (7.7)	4 (22.2)	2 (8.3)	8 (19.5)	2 (18.2)
ant decompression via pst approach & fusion	4	1 (5.9)	1 (3.6)	0	2 (11.1)	2 (8.3)	1 (2.4)	1 (9.1)
circumferential decompression & fusion	13	2 (11.8)	4 (14.3)	4 (30.8)	3 (16.7)	2 (8.3)	9 (22.0)	2 (18.2)

* ant = anterior; pst = posterior.

Preoperative and Postoperative Factors Related to Surgical Outcomes

Preoperative and postoperative factors that were potentially related to the recovery rate were assessed, including age, sex, preoperative morbidity period, preoperative JOA scale score, ossified lesion morphological type, ossified lesion anteroposterior diameter, kyphosis angle of the thoracic vertebra, presence of an intramedullary high-intensity lesion on T2-weighted MR images, maximum ossification level, surgical method, use of instrumentation, presence or absence of DM, and number of operations. The results revealed significant differences in recovery rates between patients with and without DM (Table 3). Although there was no significant difference in the recovery rate among the 4 surgical methods performed in this study, the recovery rate tended to be higher among patients undergoing anterior decompression and fusion via an anterior approach or circumferential decompression and fusion than among those undergoing posterior decompression and fusion or anterior decompression via a posterior approach and fusion.

Patient Complications

One or more complications were experienced by 31 patients (40.8%), including postoperative neurological deterioration in 20 patients (transient in 17 and permanent in 3); dural tears in 7; epidural hematomas in 5; respiratory complications in 4; instrumentation failure, deep infection, superficial infection, and vertebral fracture in 1 patient each; and other complications in 10 patients.

Postoperative neurological deterioration was observed immediately after surgery in 10 patients and from 1 day to 2 weeks after surgery in 10 patients. Postoperative neurological deterioration was observed equally in the anterior approach group and the posterior approach group (24% vs 27.5%). Participating investigators suggested the following reasons for the neurological deterioration: intraoperative trauma to the spinal cord in 9 patients, postoperative hematoma in 5, CSF leakage in 2, other reasons in 2 patients, and unknown causes in 2 patients. Surgical intervention for neurological deterioration was performed in 6 patients, including additional decompression in 3 and evacuation of the hematoma in 5 (2 patients underwent both), resulting in neurological recovery in all 6 patients. Of the 14 patients who did not undergo surgical intervention for neurological deterioration, 11 experienced spontaneous neurological recovery by an average of 12.5 days after surgery.

Discussion

In the present multicenter study, the mean recovery rate of the JOA scale scores was 45.4%, which is better than the 36.8% obtained in the previous study. There are several possible reasons for this difference. First, only patients who underwent fusion surgery were included in the present study, whereas only those who underwent decompression were included in the previous study. Surgical outcomes improved significantly with the use of instrumentation, which stabilized the thoracic spine and was able to prevent the progression of or even to correct thoracic kyphosis, and thereby enhancing spinal cord decompression. Second, only 7 spine centers with notable experience in the treatment of T-OPLL participated in this study, whereas 34 institutions with varying levels of experience participated in the previous study. A third possible reason is that the present study focused on patients with more recent surgeries as compared with those included in the previous study. Therefore, improvements in both the surgical skills of the participating surgeons, the spinal instruments, and the neurophysiological monitoring may have contributed to the better surgical outcomes in the present study.

There was no significant difference in the surgical outcomes among the 4 surgical methods in the present study. However, the recovery rate tended to be higher among patients undergoing anterior decompression and fusion via an anterior approach or circumferential decompression and fusion than among those undergoing posterior decompression and fusion or anterior decompression via a posterior approach and fusion.

An anterior approach using an extra- or transpleural approach has been recommended by several authors, as it allows for direct decompression of the spinal cord by excising or floating the OPLL.[2] However, an anterior transthoracic approach for T-OPLL is technically demanding and, because the thoracic cage is opened, may place more surgical stress on patients than a posterior approach.

Although posterior decompression and fusion provides indirect decompression, leaving the OPLL in front of the spinal cord in place, this technique is less technically demanding, is associated with a lower risk of neuro-